Ashvin Srinivasan

Codebook Design for Limited Feedback Multiple Input Multiple Output Systems

School of Electrical Engineering

Thesis submitted for examination for the degree of Master of Science in Technology.

04.09.2012

Thesis supervisor:

Prof. Olav Tirkkonen

Thesis instructor:

M.Sc. (Tech.) R-A Pitaval

Aalto University
School of Electrical
Engineering

Author: Ashvin Srinivasan

Title: Codebook Design for Limited Feedback Multiple Input Multiple Output Systems

Date: 04.09.2012   Language: English   Number of pages:8+65

Department of Communications and Networking

Professorship: Communications Engineering   Code: S-72

Supervisor: Prof. Olav Tirkkonen

Instructor: M.Sc. (Tech.) R-A Pitaval

From the past few years, there has been an exponential rise in the communication sector, especially wireless continuously fueled by the demand of higher data rates by users. The concept of multiple input multiple output (MIMO) systems is used extensively in currently deployed technologies to provide necessary data rates. MIMO systems using spatial multiplexing achieves higher data rates without wasting frequency or time resources. This happens even when there is channel state information only at the receiver. It was observed that the channel knowledge at the transmitter further increases the capacity of a system. Perfect channel state information at the transmitter(CSIT) is generally not feasible in FDD systems, however, partial CSIT may be used to further increase the capacity of a system. This is commonly referred to as precoding. In precoding, codebooks which are designed off-line and stored, known to both the transmitter and receiver, are used. The main objective of this thesis pertains to the designing of codebooks and the effect of codebooks on the capacity of limited feedback MIMO systems. A codebook contains codewords in the form of matrices and the design of these matrices reduces to a quantization problem on certain manifolds. The algorithm employed for quantizing these manifolds is the Lloyd algorithm, one of the most widely used. We make use of specific geometrical properties of these manifolds to design codebooks.

Previously, much work has been done on designing codebooks by quantizing a Grassmann manifold. Here, an alternate quantization of a permutation invariant flag manifold is considered. We derive semi analytical distortion bounds to evaluate our codebook. Through this work, codebooks thus obtained are used and their effect on capacity is observed and analyzed.

Keywords: MIMO systems, FDD systems, Channel State Information Precoding, Codebook, Vector Quantization, Lloyd Algorithm Grassmann Manifold, Permutation Invariant Flag Manifold

Acknowledgment

First and foremost, I would like to offer my sincerest gratitude to my supervisor, Prof. Olav Tirkkonen for providing me this wonderful opportunity, freedom to pursue research in the area of my interest. I am very fortunate to have such a benevolent supervisor. I would also like to thank my instructor, Renaud-Alexandre Pitaval for his guidance and timely suggestions. I thank Alex for formulating the research problem this thesis addresses without which this thesis could never have been implemented. I have learned a lot from you, it truly has been an enlightening and rewarding journey, many thanks to you.

During the course of my research, I was very fortunate to work on concepts such as manifolds, vector quantization among others. I would especially like to thank the authors: Pramod Viswanath, David Tse, Allen Gersho, Robert M.Gray, Olav Tirkkonen, Risto wichman, Ari Hottinen, Gilbert Strang, Thomas M cover, Chris J Isham, Mohinder Jankiraman, Rajesh T. Krishnamachari for their priceless contributions in the field of wireless communications.

Without my friends I could not have progressed this far! I would like to thank all my friends here and back home, especially Vijay and Narayana for their never ending support, fun conversations that got me through difficult times. Lastly, and most importantly, I would like to thank my mother, father, and Dittu who have helped and stood by me in the darkest of times.

The author alone is held accountable for the conclusions drawn from this thesis and any errors it may contain.

This thesis is the end of the road for me in obtaining my M.Sc. degree. However, the quest of learning, finding solutions is an integral part of every being! As Einstein rightly said:

" The most beautiful thing we can experience is the mysterious. It is the source of all true art and all science. He to whom this emotion is a stranger, who can no longer pause to wonder and stand rapt in awe, is as good as dead: his eyes are closed."

Otaniemi, 04.09.2012

Ashvin Srinivasan

Contents

List of Figures

List of Tables

Abbreviations

Abbreviations

CSIR	Channel State Information at the Receiver
CSIT	Channel State Information at the Transmitter
DPSK	Differential Phase Shift Key
EGC	Equal Gain Combining
FDD	Frequency Division Duplex
GLA	General Lloyd Algorithm
HSPA	High Speed Packet Access
i.i.d	independent and identically distributed
LOS	Line Of Sight
LTE	Long Term Evaluation
MIMO	Multiple Input Multiple Output
MISO	Multiple Input Single Output
MQ	Matrix Quantizer
MQE	Mean Quantization Error
MRC	Maximal Ratio Combining
MU-MIMO	Multiple User Multiple Input Multiple Output
NN	Nearest Neighbor
OFDM	Orthogonal Frequency Division Multiplexing
SIMO	Single Input Multiple Output
SISO	Single Input Single Output
SNR	Signal to Noise Ratio
SU-MIMO	Single User Multiple Input Multiple Output
SVD	Singular Value Decomposition
VQ	Vector Quantization
4G	Fourth Generation

1   Introduction

1.1   Background

Wireless communication refers to the transmission of signals across a wireless medium [1]. With the passage of time, wireless communications has changed drastically with an extensive use of communication services, thus requiring a need for more capacity. Unlike wired communications, wireless has to deal with environmental challenges such as fading and noise, with the addition of bandwidth and transmit power constraints. The increase in demand of high transmission capacity had to be fulfilled by effective usage of available bandwidth and channel conditions, One of the ways proposed was by employing multiple transmitters and multiple receivers often referred to as Multiple Input Multiple Output (MIMO) systems. MIMO wireless systems provide the necessary data rates and link range without the usage of additional bandwidth or increased transmit power, which was demonstrated by researchers at Bell labs during the mid-90s [2].

A traditional communication system consists of a single transmit and receive antenna, often referred to as a Single Input Single Output(SISO) system. This kind of system does not offer any gains besides transmission, often affected by fading. Systems like SIMO and MISO were introduced to counter this fading issue by exploiting the diversity of channel conditions, also providing array/beamforming gain. In addition to the diversity and array gains, MIMO systems exhibits multiple degrees of freedom allowing spatial multiplexing gain, leading to a significant rise in the data throughput. To gain an insight on diversity, let us consider a simple communication system in which a transmitted radio signal propagates through multiple paths before reaching the receiver, which is termed as multipath propagation. The received signal is the superposition of different multi-paths. If there is no direct line of sight (LOS), then channel coefficients of each path is assumed to be independent and identically distributed with finite mean and variance. By applying central limit theorem, the resulting channel coefficient can be modeled as a complex Gaussian random variable [3, page 8]. Often, the resulting channel coefficient has a very small gain, thus transmission may not be suitable. To counter this problem of small channel gains we make use of diversity. The different diversity schemes are time diversity, frequency diversity, and space diversity. In MIMO systems, space diversity is used. Array gain in MIMO systems result in increase of average received SNR obtained by coherently combining the incoming signals. Generally, the receiver has knowledge of the channel, this channel state information at the receiver (CSIR) is made possible by initially transmitting a pilot signal known to the receiver beforehand. Since, the pilot signal is known, the receiver estimates the channel from the received signal. The knowledge of channel at the receiver results in achieving a higher data rate. It has been observed that having knowledge about the channel at transmitter (CSIT) helps in further increase of data rate. However, at transmitter, it usually is difficult to realize the channel by employing the pilot signal method as the uplink and downlink are of different frequencies (FDD) [4]. Thus, we resort to partial-CSIT, facilitated by the feedback of some information about the channel properties from

the receiver. A predefined codebook (a set of code words) is known to transmitter and the receiver as well, the codebook contains information about the quantized CSI in the form of precoding matrices. The receiver quantizes the channel state information and feed them back by transmitting an index of the selected codeword chosen from the codebook. It is because of the above mentioned advantages and versatility, MIMO is an integral part of many wireless communication standards such as IEEE 802.11n (Wi-Fi), 4G, Wimax, Long Term Evaluation (LTE), HSPA+.

1.2 Resarch problem and scope

Partial channel state information at the transmitter increases the throughput of a system. In order to achieve this throughput increase, we consider transmit precoding in which we use predetermined codebooks designed off-line, known to both ends of a system. By orthogonalization of data streams and transmitting them along Eigen-dimensions, these codebooks reduce cross talk impacting the system throughput. The objective of this thesis is to construct codebooks for limited feedback MIMO systems by considering unitary precoding in which we introduce a quantization scheme on a specific flag manifold using modified Lloyd algorithm. The analysis of the codebook is based on volume of a metric ball in the given manifold. We derive the volume formula using numerical methods, and obtain semi-analytical upper and lower distortion bounds. The scope of this thesis lies in the impact of our codebook on the system capacity.

1.3 Thesis outline

This thesis is divided into two parts. The first part contains literature review while the second part pertains to the analysis of our numerical results. The first part is presented in sections 2, 3, and 4. The second part is discussed in detail in sections 5, and 6.

- Section 2 gives an overview of MIMO technology which forms the basis for this thesis. Important features like diversity and spatial multiplexing gains of a system are discussed. Fundamental theoretical concepts on capacity are also presented.

- The notion of manifolds is introduced in Section 3. Relevant concepts like tangent spaces, exponential mapping are discussed briefly. The concept of Riemannian and Grassmann manifold are also presented which are essential for our codebook design.

- Section 4 is about precoding, necessity and brief description of limited feedback systems. Relevant vector quantization concepts are discussed. Section 4 basically connects the objectives of section 2 and 3, directly addressing our research problem.

- A thorough analysis of Lloyd algorithm specific to this thesis is presented. Semi-analytical bounds for second order distortion are obtained, Monte Carlo

simulations of codebook performance along with the bounds are presented in Section 5. The codebooks' quality is analyzed in detail.

- We analyze and discuss the impact of using our codebooks on the capacity of a limited feedback system equipped with a linear ZF receiver in Section 6, which is thus shown to be a good solution to the proposed problem.

2 MIMO wireless systems

This section reviews the evolution of a simple communication system i.e. SISO to MIMO, benefits of deploying MIMO systems, and environmental factors that affect MIMO capacity. Furthermore, we define and investigate on some basic properties of a MIMO transmission model. Since capacity is one of the key parameters in this thesis, we discuss about the necessary information theoretic concepts which provide the information required for better understanding of MIMO technology. With background knowledge of MIMO technology, we take a closer look at the already mentioned diversity and array gain.

2.1 Prior work and Motivation

Wireless communication has its fundamentals based on Electromagnetic theory proposed by James Clark Maxwell. The first long range transatlantic radio link was established by Marconi in 1901, since then wireless communication has advanced drastically. Initially wireless was about analogue phones and radio paging, nowadays, global connectivity is made possible by advanced wireless technologies. We can communicate with each other in a matter of seconds using our mobile phones or personal communication devices. The simplest form of a wireless communication model is having a single antenna at the transmitter and at the receiver as well, it is sometimes referred as SISO.

Figure 1: SISO transmission model.

The signal x(t) is transmitted in the air and y(t) received. Given all the details of the reflectors and absorbers in the environment, one can use Maxwell's equations to find out the propagation of the electromagnetic waves and get y(t) as an exact function of x(t). However, we do not need such rigorous calculation to obtain the model. The transmitter and the receiver antennas are usually separated by several wavelengths and far field approximations of signal propagation is good enough to obtain a model that is applicable to most of the surroundings [5].

Let us focus on a familiar Additive White Gaussian Noise(AWGN) channel.

where $x[m]$ and $y[m]$ are real input and output at time m respectively and $w[m]$ is $\mathcal{N}(0, \sigma^2)$. noise, independent over time. It is very essential to mention this channel as this will be a basic building block for the subsequent wireless channels mentioned in this thesis [1, page 167].
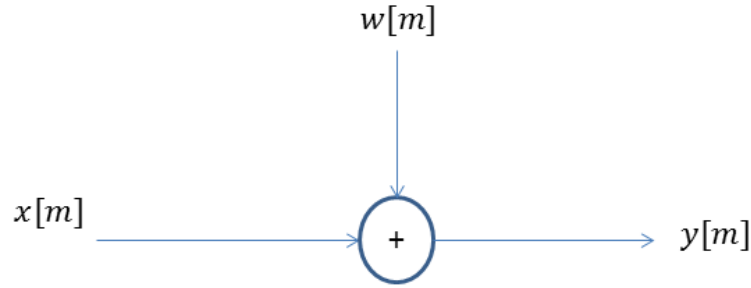
Figure 2: channel model 1

The input and output is related as

$$y[m] = x[m] + w[m] \tag{1}$$

We can model the EM signals as rays. Each ray experiences a certain amount of propagation delay and attenuation. Further, the rays get reflected by different reflectors present in the surrounding environment. Thus, the signal arrives via multiple paths, each having its own delay and attenuation. Our final model contains signal subjected to a channel along with AWGN. The channel model 1 is modified to
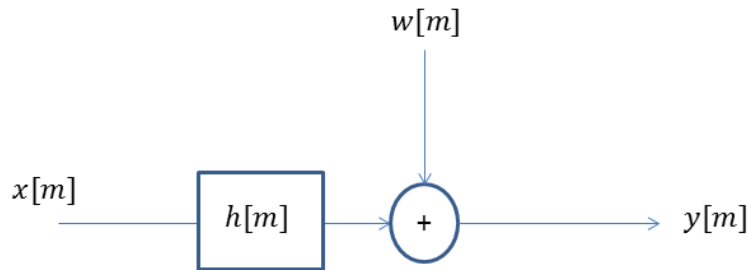
Figure 3: channel model 2

(1) is modified to be

$$y[m] = \sum_i a_i x(m - \tau_i) + w[m] \tag{2}$$

Where a_i is the attenuation coefficient of the ith path and τ_i is the delay it experiences.

Rayleigh fading

Most often, in a typical mobile radio channel, the mobile unit receives the signal via multiple paths with no direct line of sight. When the number of paths is large, by applying the central limit theorem , the resulting channel coefficient can be modeled as a complex Gaussian random variable with zero mean and finite variance. Thus, the envelope of the received signal follows a Rayleigh probability distribution and its phase follows obeys a uniform distribution between $-\pi$ to π [6, page 51]. The probability distribution function of Rayleigh distribution is given by

$$p(a) = \begin{cases} \frac{a}{\sigma_s^2} e^{\frac{-a^2}{2\sigma_s^2}} & \text{if } a \geq 0; \\ 0 & \text{if } a < 0. \end{cases}$$

If there is a direct line of sight then we can model the channel based on Rician fading. In our subsequent sections, we assume that the channel experiences flat-fading. Thus, a single filter tap is sufficient to represent the channel. The channel is given by

$$h[m] = \sum_i a_i \delta(m - \tau_i) \tag{3}$$

We can now modify (2) as

$$y[m] = h[m].x[m] + w[m] \tag{4}$$

The above explained model is SISO, the simplest antenna technology. In some environments, SISO systems are vulnerable to problems caused by multipath effects. The signals coming from different paths causes problems such as fading, cut-out(cliff effect), and intermittent reception(picket fencing). In a real time situation, for a given digital communication system, these problems can cause a reduction in the data throughput and an increase in the error rate.

In order to mitigate the problems caused by multipath wave propagation, smart antenna technology is used. There are three forms of smart antenna, known as SIMO(single input, multiple output), MISO(multiple input, single output), and MIMO(multiple input, multiple output).

2.2   SIMO systems

Let us consider a SIMO channel with one transmit antenna and n_R receive antennas as Figure 4

The output at the receiver is given by

$$y_l[m] = h_l x[m] + w_l[m] \quad l = 1, ..., n_R, \tag{5}$$

where h_l is the fixed(invariant for a small time duration) complex channel gain from the transmit antenna to the lth receive antenna, and $w_l[m]$ is $\mathcal{CN}(0, \sigma^2)$, is the additive white Gaussian noise. A sufficient statistic needed to obtain $x[m]$ from $\boldsymbol{y}[m] = [y_1[m], y_2[m], ..., y_{n_R}[m]]^t$ is [1, Page 179]
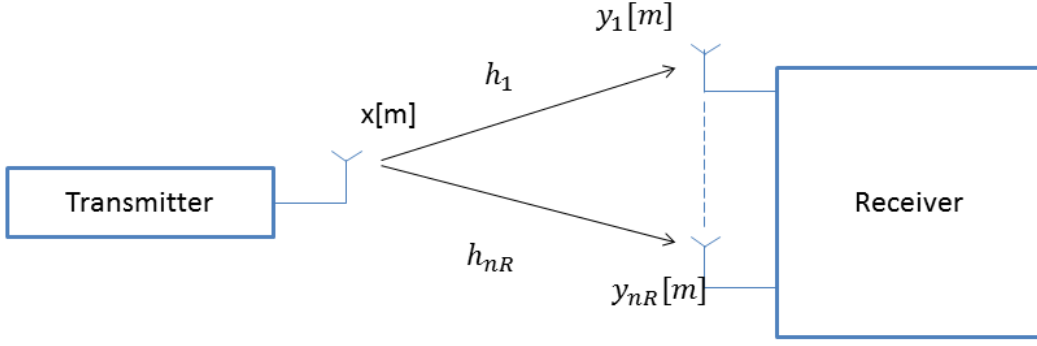
Figure 4: SIMO transmission model.

$$\tilde{y}[m] = \boldsymbol{h}^* \boldsymbol{y}[m] = \boldsymbol{h}^* \boldsymbol{h} x[m] + \boldsymbol{h}^* \boldsymbol{w}[m], \tag{6}$$

where $\boldsymbol{h} = [h_1, ..., h_{n_R}]^t$ and $\boldsymbol{w}[m] = [w_1, ..., w_{n_R}]^t$. This is an AWGN channel with

$$SNR(\gamma) = \frac{P|\boldsymbol{h}^* \boldsymbol{h}|^2}{\mathcal{E}\{|\boldsymbol{h}^* \boldsymbol{w}|^2\}}, \tag{7}$$

where P is the average power per transmit symbol.

The noise power is given by

$$P_n = \mathcal{E}\{|\boldsymbol{h}^* \boldsymbol{w}|^2\} = \mathcal{E}\{|\boldsymbol{h}^* \boldsymbol{w} \boldsymbol{w}^* \boldsymbol{h}|\} = \boldsymbol{h}^* \mathcal{E}\{\boldsymbol{w} \boldsymbol{w}^*\} \boldsymbol{h} = \sigma^2 \boldsymbol{h}^* \boldsymbol{I}_{n_R} \boldsymbol{h} = \sigma^2 \boldsymbol{h}^* \boldsymbol{h}.$$

Where $\boldsymbol{I}_{n_R}$ is n_R by n_R identity matrix. (6) and (7) becomes

$$\gamma = P \frac{|\boldsymbol{h}^* \boldsymbol{h}|^2}{\sigma^2 \boldsymbol{h}^* \boldsymbol{h}} = P \frac{\boldsymbol{h}^* \boldsymbol{h}}{\sigma^2} = P \frac{||\boldsymbol{h}||^2}{\sigma^2}, \tag{8}$$

and

$$\tilde{y}[m] = \boldsymbol{h}^* \boldsymbol{y}[m] = ||\boldsymbol{h}||^2 x[m] + \boldsymbol{h}^* \boldsymbol{w}[m] \tag{9}$$

respectively. The capacity is given by

$$C = \log_2 \left(1 + \frac{P_s ||\boldsymbol{h}^2||}{\sigma^2} \right) \text{ bits/s/Hz.} \tag{10}$$

We have to keep in mind that the weight at each receiver antenna is assumed to be it's corresponding fading channel amplitude. This assumption is made in order to have a clear understanding on how diversity combats fading which is reflected in (8), maximizing the output SNR by having channel gain($||\boldsymbol{h}||^2$). However, in reality the weighting factors are estimated by using diversity schemes.

We use receive diversity scheme by having multiple receive antennas to maximize the SNR, also known as diversity gain. The central idea here is that antennas receive

different versions of the same signal. The probability of all these copies being in a deep fade is considerably small. However, employing diversity schemes makes sense only when the fading is independent from element to element. In general, the performance of the communication system with diversity techniques depends on the way the multiple signal replicas are combined at the receiver in order to improve the overall SNR. The different types of combining methods used at the receiver are selection combining, maximal ratio combining, and equal gain combining. The goal of all these diversity schemes is to find a set of weights $\boldsymbol{\alpha}$, which are chosen to mitigate the fading effect for a single user.

2.2.1 Selection Combining

Selection combining is a simple diversity combining method, the block diagram for selection combining is as shown in Figure 5. In such a system, the largest instantaneous signal to interference ratio is selected as the output.
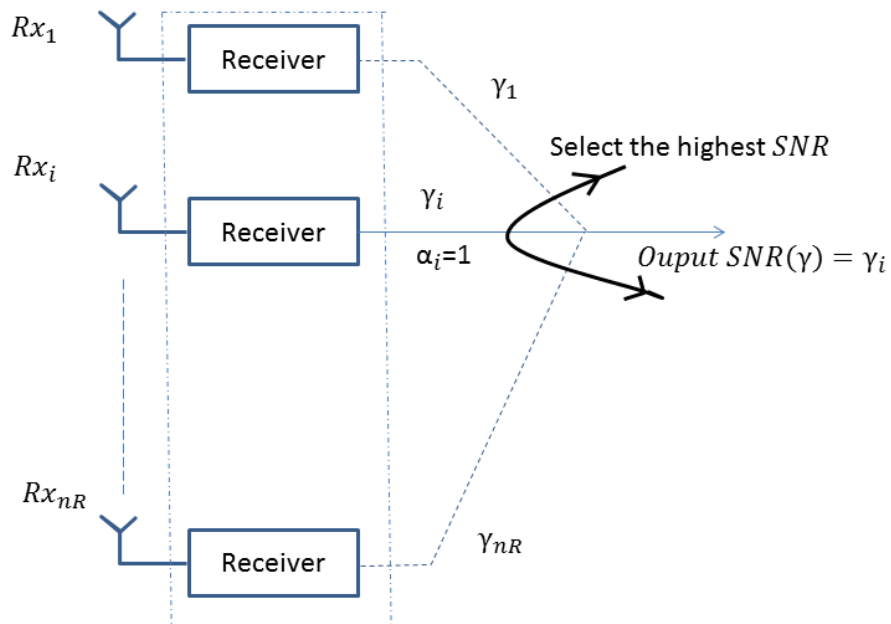
Figure 5: Selection combining method

In selection combining therefore,

$$\alpha_i = \left\{ \begin{array}{ll} 1 & \gamma_i = \max_n\{\gamma_n\}; \\ 0 & \text{otherwise,} \end{array} \right\}$$

Since the antenna chosen is the one with maximum SNR, the output SNR of the selection diversity scheme is $\gamma = max_n\{\gamma_n\}$.

2.2.2   Maximal Ratio Combining

In selection diversity scheme, the antenna having the best SNR is chosen. This is not the optimal solution since $n_R - 1$ antennas are completely ignored. Maximal ratio combining(MRC) is a linear combining method, in which various signals are individually weighted and then summed together in order to maximize the output SNR. The block diagram is as shown in Figure 6.
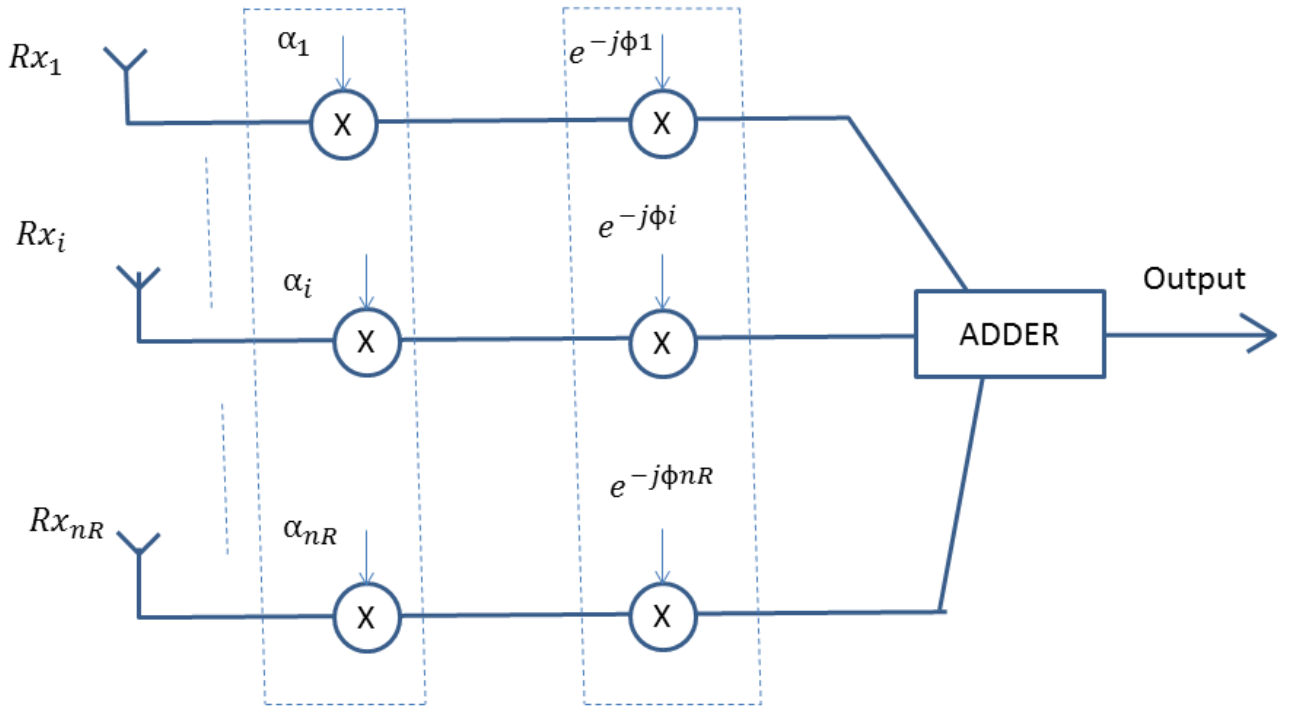
Figure 6: Maximal Ratio Combining with weighting factors followed by co-phasing

The output signal from an MRC scheme is given by

$$\tilde{y}[m] = \boldsymbol{\alpha}^* \boldsymbol{y}[m], \tag{11}$$

The SNR is given by $\gamma = P|\boldsymbol{\alpha}^*\boldsymbol{h}|^2/\sigma^2\boldsymbol{\alpha}^*\boldsymbol{h}$. By the Cauchy-Schwarz inequality [7, page 4-6], γ attains the maximum when $\boldsymbol{\alpha}$ is linearly dependent on $\boldsymbol{h}$, i.e.,

$$\boldsymbol{\alpha} = \boldsymbol{h}.$$

Thus,

$$\gamma = P\frac{|\boldsymbol{h}^*\boldsymbol{h}|^2}{\sigma^2\boldsymbol{h}^*\boldsymbol{h}} = P\frac{||\boldsymbol{h}||^2}{\sigma^2} = P\sum_{n=0}^{n_R-1}\frac{|h_n|^2}{\sigma^2} \tag{12}$$

The maximum diversity can be achieved when the weights are the same as the channel coefficients. This method is called optimum combining since it maximizes

the output SNR, and the data throughput achieved will be the capacity(Shannon's limit) of the system as observed in (10).

2.2.3   Equal Gain Combining

Equal gain combining(EGC) is a sub-optimal but simple linear diversity combining technique. MRC is optimal in the sense of maximizing SNR, however, the weights should adapt with respect to the fading signals, whose amplitude may fluctuate with time. This is avoided in the case of EGC by setting amplitudes of the weighting factors to be unity. Thus, we have

$$\alpha_n = e^{j \arg(h_n)}$$

.

In this manner the signals coming from each individual branch is cophased and added together. The implementation of EGC is relatively easy as it does not require estimation of the fading amplitude. However, the downside is that the performance is EGC is less than that of MRC.

2.3   MISO systems

Let us consider a MISO system Figure 7 with n_T transmit antennas and one receive antenna
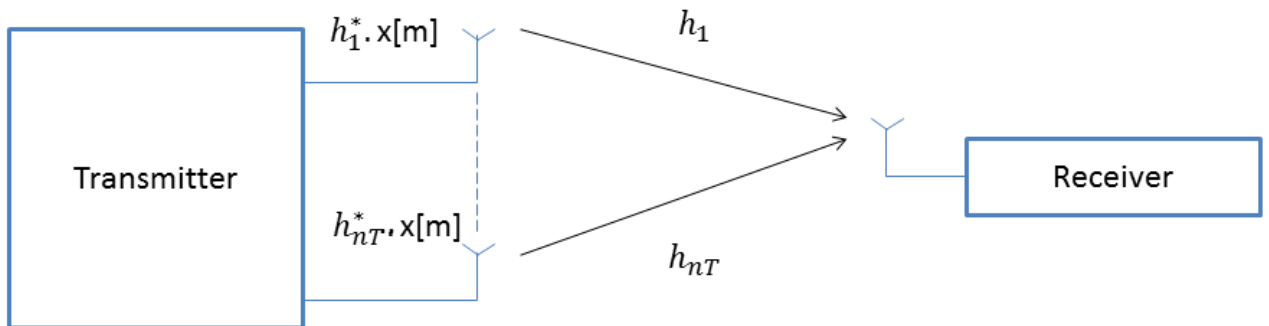
Figure 7: MISO transmission model.

$$y[m] = \boldsymbol{h}^* \boldsymbol{x}[m] + w[m], \tag{13}$$

where $\boldsymbol{x}[m]$ is the vector containing the transmitted symbol $\tilde{x}[m]$. The channel is considered to be slow fading and is assumed to be known at the transmitter to gain an insight on the capacity of the system, power gain via transmit diversity. $\boldsymbol{h} = [h_1, ..., h_{n_T}]^t$ and h_{n_T} is the channel gain from the transmit antenna n_T to the receive antenna. In the previous mentioned SIMO channel, the statistic which was required was the projection of n_R along the channel as shown in (9). Thus, an

intuitive way for the MISO channel is to send the signal along the channel vector $\boldsymbol{h}$ [1, page 180]. Thus,

$$\boldsymbol{x}[m] = \frac{\boldsymbol{h}}{||\boldsymbol{h}||}\tilde{x}[m],$$

where $\boldsymbol{h}/||\boldsymbol{h}||$ is the matched filter used at the transmitter. (13) reduces to a simple AWGN channel of the form

$$\boldsymbol{y}[m] = ||\boldsymbol{h}||\tilde{x}[m] + w[m] \tag{14}$$

with a total power constraint P_s. The capacity is given by

$$C = \log_2\left(1 + \frac{P_s||\boldsymbol{h}^2||}{\sigma^2}\right) \text{bits/s/Hz.} \tag{15}$$

Multiple antennas are used at the base station for uplink receive diversity in order to compensate for the low power signal transmitted from the mobile terminal. But, using multiple antennas at the mobile terminal during downlink receive diversity is not recommended. Since, increasing the number of antennas at the mobile terminal results in more processing power, which is limited for a mobile. Thus, we have multiple antennas at the base station and employ transmit diversity schemes for downlink.

The transmission diversity maximizes SNR when the signals received from different transmit antennas are added coherently and more power is allocated to those channels with better channel gain. This method of steering the transmit signal in the direction of transmit antenna array pattern is often referred to as transmit beamforming [1, page 180] . Many transmit diversity schemes have been proposed in the past. The schemes are basically of two types: schemes with and without feedback. The difference in these two schemes is that the former has the channel knowledge at the transmitter obtained via feedback channel, while the latter has no channel knowledge and aims to achieve diversity by using space-time codes [8] [9] .

In the case of transmit diversity with feedback, the weighting factors is chosen in a such a way so as to maximize the SNR or the channel capacity. One such example is switched diversity proposed for DPSK mobile radio systems [10]. Sometimes, in practical mobile systems, channel estimation is difficult due to the mobility and environment. This imperfect channel estimation can have an adverse affect on the system performance. Thus, sometimes space-time codes are used at the transmitter, which do not require any channel knowledge. Space-time trellis codes, linear space-time block codes are some examples of space-time codes. An in-depth analysis of space-time codes is beyond the scope of this thesis. (10) and (15) clearly shows the effect of receive and transmit diversity on power gain respectively.

In the SIMO and MISO examples, the benefit of having multiple antennas either at the receiver or transmitter side results only in power gain. To get a gain in degrees of freedom, one has to use multiple transmit and multiple receive antennas. The degrees of freedom of a channel is the dimension of the received signal space. It has been shown in [2, 11] that number of degrees of freedom for a single-user point to

point MIMO($n_T \times n_R$) channel is $n_S = min(n_T, n_R)$.

2.4 MIMO wireless systems

We will see that under suitable channel conditions, having both multiple transmit and multiple receive antennas provides an additional spatial dimension for communication and yields a degree of freedom gain. Because of these additional degrees of freedom, we can break down a high data rate signal into multiple low data rate signals(so called streams) and transmit them from each of the multiple transmit antennas. Thus, the space dimension is multiplexed and it is commonly referred to as *spatial multiplexing*.

In a $n_T \times n_R$ MIMO, the maximum spatial multiplexing order i.e. the number of streams is limited to

$$n_S = \min(n_T, n_R),$$

(or rank of the MIMO channel matrix $\boldsymbol{H}$) if a linear receiver is used. This means that n_S streams can be transmitted in parallel, theoretically leading to an n_S times increase of the capacity. However, the spatial multiplexing gain is limited due to spatial correlation, since some of the channel coefficients may be correlated leading to weak channel gains.

2.4.1 MIMO system model

We consider a single user communication and a point-to-point link where the transmitter is equipped with n_T antennas and receiver with n_R antennas. We also assume that bandwidth of the message signal is less than coherence bandwidth of the channel, i.e. all frequency components of the signal experience the same magnitude of fading(flat fading). If the channel is frequency selective then one could use an orthogonal frequency division multiplexing (OFDM) system to turn the MIMO channel into a set of parallel frequency-flat MIMO channels [12].

We shall consider a narrow band, block fading (time invariant for certain symbol intervals L) channel in order to get the under lying structure of a MIMO system model as shown in Figure 8

where $h_{i,j}$ is the path gain from transmit antenna j to receive antenna i. let the complex valued signals $\{x_1, ..., x_{n_T}\}$ be transmitted thorough n_T antennas respectively. The received signal at the ith antenna is

$$y_i = \sum_{j=1}^{n_T} h_{i,j} x_j + w_i, \tag{16}$$

The channel path gains, transmitted complex valued signals, and the received signals for the system model can be represented as
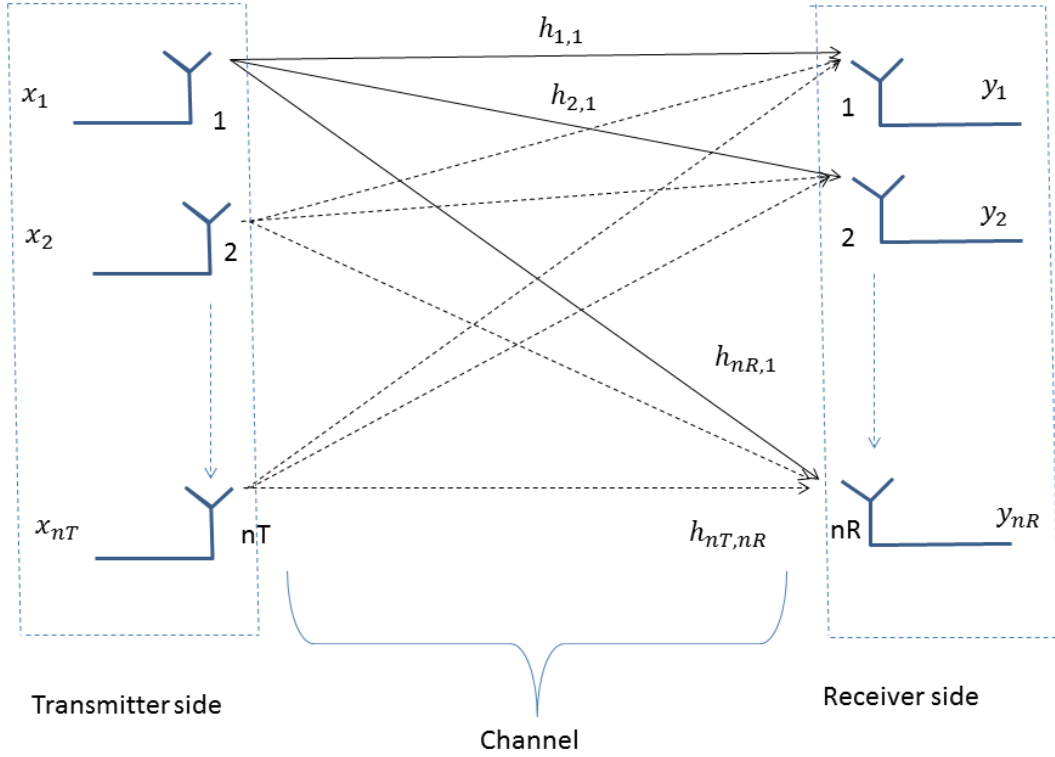
Figure 8: MIMO system model.

$$\boldsymbol{H} = \begin{bmatrix} h_{1,1} & h_{1,2} & \dots & h_{1,n_T} \\ h_{2,1} & h_{2,2} & \dots & h_{2,n_T} \\ \vdots & \vdots & \ddots & \vdots \\ h_{n_R,1} & h_{n_R,2} & \dots & h_{n_R,n_T} \end{bmatrix},$$

$$\boldsymbol{x} = [x_1, ..., x_{n_T}]^t \quad \boldsymbol{x} \in \mathcal{C}^{n_T},$$

$$\boldsymbol{y} = [y_1, ..., y_{n_R}]^t \quad \boldsymbol{y} \in \mathcal{C}^{n_R},$$

respectively. Thus, (16) [3, page 6-7] can be extended to

$$\boldsymbol{y} = \boldsymbol{H}\boldsymbol{x} + \boldsymbol{w}. \tag{17}$$

The noise vector

$$\boldsymbol{w} = [w_1, w_2, ..., w_{n_R}]^t \in \mathcal{C}^{n_R}$$

where $\boldsymbol{w}$ is assumed to be spatially white circular Gaussian random variable(for reasons explained later) with zero mean and finite variance, i.e.

$$\boldsymbol{w} \sim \mathcal{CN}(0, \sigma_n^2 \boldsymbol{I})$$

.

The transmitted signal satisfies the total power constraint:

$$\mathcal{E}(\boldsymbol{x}^*\boldsymbol{x}) = \sum_{i=1}^{n_T} \mathcal{E}\left(|x_i|^2\right) = \sum_{i=1}^{n_T} \sigma_{s,i}^2 \leq P_s.$$

Since the channel remains constant for L symbol intervals(block fading), we can further extend (17) [3, page 7] to

$$\boldsymbol{Y} = \boldsymbol{HX} + \boldsymbol{W} \tag{18}$$

where $\boldsymbol{Y} = [\boldsymbol{y}_1, ..., \boldsymbol{y}_L]$, $\boldsymbol{X} = [\boldsymbol{x}_1, ..., \boldsymbol{x}_L]$, and $\boldsymbol{W} = [\boldsymbol{w}_1, ..., \boldsymbol{w}_L]$.

2.4.2   Information theory background

In this section, we discuss the information theory behind the capacity expressions used throughout the thesis, and for analysis of MIMO systems. Furthermore, these concepts are essential for analyzing the results obtained in the final chapter. Information theory is a vast branch of applied mathematics and electrical engineering, thus, only the necessary basic concepts have been explained. For the following definitions and concepts, we have referred to [13, page 183,184], [3, page 10-12]. However, We have not elucidated any proofs.

Information theory was developed by Claude E. Shannon to find fundamental limits on signal processing operations such as data compression and ultimate transmission rate of any communication system. In order to find the ultimate transmission rate(or capacity of a system), we initially need to explain the communication process.
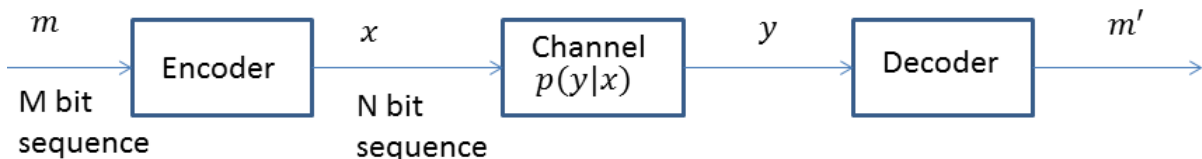
Figure 9: General communication system,

A typical communication system is shown in Figure 9. Let us assume that original message 'm'(M bit sequence) is first mapped into a longer message 'x'(N bit sequence) via a encoder with $N > M$, the extra bits are added to compensate for transmission errors. The encoded message x is sent through a communication channel and the output message from the channel is 'y'. The channel is defined

by the transition probability $p(y|x)$, i.e. the probability that the received signal is y subjected to the condition of transmitted signal being x. In a noiseless channel, the message received is $y = x$. But, in the case of a noisy channel, y is generally different from x. Though y is random, it still has a distribution that depends on x. Hence, from y, the decoder deduces an estimate, m' of the original message.

The following definitions are from [13, page 191-192, 200-201]

Channel capacity: *We have a discrete channel consisting of input alphabet $\mathcal{X}$ and output alphabet $\mathcal{Y}$ and a probability transition matrix $p(y|x)$ that expresses the probability of observing the output symbol* y *given that we send the symbol* x. *The channel is said to be memoryless if the probability distribution of the output depends only on the input at that time and is conditionally independent of previous channel inputs or outputs. Thus we define the channel capacity of a discrete memoryless channel as*

$$C = \max_{p(x)} I(X;Y).$$

Where the maximum is taken over all possible input distributions $p(x)$

The prior definition of capacity is needed for the recap of Shannon's second theorem which gives a view of channel capacity as the highest rate at which the information can be transmitted (in bits per channel use) with a low probability of error.

Shannon's second law: *The total number of possible Y sequences is $\approx 2^{nH(Y)}$. This set has to be divided into sets of size $2^{nH(Y|X)}$ corresponding to the different input X sequences. The total number of disjoint sets is less than or equal to $2^{n(H(Y)-H(Y|X))} = 2^{nI(X;Y)}$. Hence, at most $2^{nI(X;Y)}$ distinguishable sequences of length n can be sent.*

Having familiarized with the concept of channel capacity, we now state the basic theorem in information theory.

Channel coding theorem: *For a discrete memory less channel, all rates below capacity* C *are achievable. Specifically, for every rate* R < C*, there exists a sequence of $(2^{nR}, n)$ codes with maximum probability of error $\lambda(n) \longrightarrow 0$. Conversely, any sequence of $(2^{nR}, n)$ codes with $\lambda^{(n)} \longrightarrow 0$ must have* R $\leq$ C.

2.5 MIMO information theoretic capacity

With the basic background in information theory, we now apply these concepts to analyze MIMO wireless systems. In this following section we obtain the expressions

for MIMO capacity for deterministic and random channel. We also analyze their properties which lays the foundation for rest of the thesis.

2.5.1 Capacity of Deterministic MIMO channel

We consider a deterministic block fading channel, i.e., the channel $\boldsymbol{H}$ is assumed to be constant for L symbol intervals. This channel is described by (17) To find the channel capacity from the definition, we need the following lemmas [2]

Lemma 1: *Suppose the complex random vector is zero mean and satisfies $\mathcal{E}[\boldsymbol{xx}^*] = \boldsymbol{Q}$. Then the entropy of $\boldsymbol{x}$ satisfies $H(\boldsymbol{x}) \leq \log_2 \det(\pi e \boldsymbol{Q})$ with equality if and only if $\boldsymbol{x}$ is a circularly symmetric complex Gaussian with*

$$\mathcal{E}[\boldsymbol{xx}^*] = \boldsymbol{Q}.$$

.

That is, entropy of $\boldsymbol{x}$ is maximized only when $\boldsymbol{x}$ is a circularly symmetric complex Gaussian random variable

Lemma 2: *if $\boldsymbol{x} \in \mathcal{C}^n$ is a circularly symmetric complex Gaussian then so is $\boldsymbol{y} = A\boldsymbol{x}$ for any $A \in \mathcal{C}^{mxn}$.*

Lemma 3: *if $\boldsymbol{x}$ and $\boldsymbol{y}$ are independent circularly symmetric complex Gaussians then $\boldsymbol{z} = \boldsymbol{x} + \boldsymbol{y}$ is also circularly symmetric complex Gaussian.*

According to the channel capacity definition, the capacity of the MIMO channel is

$$C = \max_{p(x)} I(\boldsymbol{x}; \boldsymbol{y}).$$

The mutual information

$$I(\boldsymbol{x}; \boldsymbol{y}) = H(\boldsymbol{y}) - H(\boldsymbol{y}|\boldsymbol{x}) \tag{19}$$

where $H(\boldsymbol{y})$ is the differential entropy of the received vector $\boldsymbol{y}$, while $H(\boldsymbol{y}|\boldsymbol{x})$ is the conditional differential entropy of the vector $\boldsymbol{y}$, given the knowledge of input vector $\boldsymbol{x}$. From entropy of the sum of two random variables, we have $H(\boldsymbol{y}/\boldsymbol{x}) = H(\boldsymbol{w}/\boldsymbol{x})^1$. Since the vectors $\boldsymbol{x}$ and $\boldsymbol{w}$ are statistically independent, $H(\boldsymbol{y}|\boldsymbol{x}) = H(\boldsymbol{w})$, we can state (19) as

$$I(\boldsymbol{x}; \boldsymbol{y}) = H(\boldsymbol{y}) - H(\boldsymbol{w}) \tag{20}$$

and therefore maximization of mutual information $I(\boldsymbol{x}; \boldsymbol{y})$ reduces to maximizing $H(\boldsymbol{y})$. Since noise is assumed to be circularly symmetric Gaussian random and from Lemma1 we have

$$H(\boldsymbol{w}) = \log_2 \det(\pi e \boldsymbol{R}_{nn}) = \log_2 \det(\pi e \boldsymbol{I}_{n_R})$$

---

[1] If x and y are 2 r.v. drawn from 2 different sources and $z = x + y$ then $H(z/x) = H(y/x)$.

we have $\boldsymbol{x}$ with zero mean and covariance $\mathcal{E}[\boldsymbol{x}^*\boldsymbol{x}] = \boldsymbol{Q}$, then it follows from lemma1 that entropy of $\boldsymbol{y}$ is maximized when it is circularly symmetric complex Gaussian, which is the case(lemmas 2 and 3) since $\boldsymbol{x}$ is circularly symmetric Gaussian random. We first need to evaluate the covariance matrix of $\boldsymbol{y}$ in order to obtain the maximum entropy of $\boldsymbol{y}$ and thus capacity.

The covariance matrix of $\boldsymbol{y}$, $\boldsymbol{R}_{yy}$ is

$$\boldsymbol{R}_{yy} = \mathcal{E}\{\boldsymbol{yy}^*\} = \mathcal{E}\{(\boldsymbol{Hx} + \boldsymbol{w})(\boldsymbol{Hx} + \boldsymbol{w})^*\} = \mathcal{E}\{\boldsymbol{Hxx}^*\boldsymbol{H}^*\} + \mathcal{E}\{\boldsymbol{ww}^*\},$$

which can be further simplified into [3, page 13]

$$\boldsymbol{R}_{yy} = \boldsymbol{H}\mathcal{E}\{\boldsymbol{xx}^*\}\boldsymbol{H}^* + \mathcal{E}\{\boldsymbol{ww}^*\} = \boldsymbol{HQH}^* + \sigma_n^2\boldsymbol{I}_{n_R}$$

Thus, we have the maximum differential entropies of $\boldsymbol{y}$ and $\boldsymbol{w}$

$$\boldsymbol{H}(\boldsymbol{y}) = \log_2 \det(\pi e \boldsymbol{R}_{yy}) \tag{21}$$

and

$$\boldsymbol{H}(\boldsymbol{w}) = \log_2 \det(\pi e \sigma_n^2 \boldsymbol{I}_{n_R}) \tag{22}$$

respectively.

Thus using (21) and (22), we define the capacity as

$$C = \max_{p(x)} I(\boldsymbol{x}; \boldsymbol{y}) = \max_{Tr(\boldsymbol{Q} \leq P_s)} \log_2 \det(\boldsymbol{I}_{n_R} + \frac{1}{\sigma_n^2}\boldsymbol{HQH}^*) \tag{23}$$

The capacity C in (23) represents the data rate per unit bandwidth that can be transmitted reliably over the MIMO link, in other words error free spectral efficiency.

If the channel is unknown to the transmitter then the input vector $\boldsymbol{x}$ is statistically independent [14, page 23-26], covariance matrix of the input signal $\boldsymbol{Q}$ becomes an Identity matrix $\boldsymbol{I}_{n_T}$. From (23), we have[2]

$$\tilde{C} = \log_2 \det(\boldsymbol{I}_{n_R} + \frac{P_s}{n_S \sigma_n^2}\boldsymbol{HH}^*). \tag{24}$$

The matrix $\boldsymbol{HH}^* \in \mathcal{C}^{n_R \times n_R}$ is a positive semi-definite matrix whose Eigen decomposition yields

$$\boldsymbol{U\Sigma U}^*,$$

where $\boldsymbol{U} \in \mathcal{C}^{n_R \times n_R}$ is a unitary matrix and $\boldsymbol{\Sigma} = diag\{\sigma_1, ..., \sigma_{n_R}\}$ are the ordered Eigen values. The squared singular values λ_i^2 of the channel matrix $\boldsymbol{H}$ are the Eigen values of $\boldsymbol{HH}^*$.

Thus, (24) can be further simplified to

$$\tilde{C} = \log_2 \det(\boldsymbol{I}_{n_R} + \frac{P_s}{n_S \sigma_n^2}\boldsymbol{U\Sigma U}^*). \tag{25}$$

---

[2] The power term is scaled by a factor of n_S since there is no waterfilling, power is distributed equally.

We have from [15, Page 416]

$$\det(\boldsymbol{I}_{n_R} + \boldsymbol{M}\boldsymbol{N}) = \det(\boldsymbol{I}_{n_T} + \boldsymbol{N}\boldsymbol{M})$$

for matrices

$$\boldsymbol{M} \in \mathcal{C}^{n_R X n_T}$$

and

$$\boldsymbol{N} \in \mathcal{C}^{n_T X n_R}$$

. Thus, (25) reduces to

$$\tilde{C} = \log_2 \det(\boldsymbol{I}_{n_T} + \frac{P_s}{n_S \sigma_n^2}\boldsymbol{\Sigma}), \tag{26}$$

The capacity in (26) is denoted as $\tilde{C}$ since it is not the channel capacity of the system, $\tilde{C}$ can be increased when the channel knowledge is available at the transmitter.

The channel estimation at the transmitter side is usually difficult since most of the systems are FDD in nature. However, there are ways to acquire CSI at the transmitter, one of them being precoding which is discussed in detail in section 4. For the time being, we assume the channel knowledge is perfectly available at the transmitter for capacity analysis.

With the knowledge of CSI at the transmitter, we can increase the capacity by allocating different levels of power(*water filling principle*) to various transmit antennas based on different path gains. We perform Singular Value Decomposition(SVD)(See Appendix) of $\boldsymbol{H}$ to get.

$$\boldsymbol{H} = \boldsymbol{U}\boldsymbol{\Lambda}\boldsymbol{V}^* = \sum_{i=1}^{n_S} \lambda_i \boldsymbol{u}_i \boldsymbol{v}_i^* \tag{27}$$

.

Where $\boldsymbol{U} \in \mathcal{C}^{n_R \times n_R}$, $\boldsymbol{V} \in \mathcal{C}^{n_T \times n_T}$ satisfying

$$\boldsymbol{U}\boldsymbol{U}^* = \boldsymbol{U}^*\boldsymbol{U} = \boldsymbol{I} = \boldsymbol{V}\boldsymbol{V}^* = \boldsymbol{V}^*\boldsymbol{V}$$

thus,

$$\boldsymbol{H}\boldsymbol{H}^* = [\boldsymbol{U}\boldsymbol{\Lambda}\boldsymbol{V}^*][\boldsymbol{V}\boldsymbol{\Lambda}\boldsymbol{U}^*] = [\boldsymbol{U}\boldsymbol{\Lambda}^2\boldsymbol{U}^*].$$

where $\boldsymbol{\Lambda} \in \mathcal{R}^{n_R X n_T}$, non diagonal entries are zero, and diagonal entries $\lambda_1 \geq \lambda_2 \geq$ ...... $\geq \lambda_{n_S}$ are the ordered singular values of channel matrix $\boldsymbol{H}$. Let us consider a input vector $\tilde{\boldsymbol{x}} \in \mathcal{C}^{n_S}$, this vector $\tilde{\boldsymbol{x}}$ is pre multiplied with the matrix $\boldsymbol{V}$ before transmission. The signal vector received $\boldsymbol{y}$ is post multiplied by $\boldsymbol{U}^*$ by using a simple receiver, i.e.,

$$\boldsymbol{x} = \boldsymbol{V}\boldsymbol{Q}\tilde{\boldsymbol{x}}$$

$$\tilde{\boldsymbol{y}} = \boldsymbol{U}^*\boldsymbol{y}$$

$$\tilde{\boldsymbol{w}} = \boldsymbol{U}^*\boldsymbol{w}$$

The input output relation given in (17) can be restated as

$$\tilde{y} = U^*HVQ\tilde{x} + U^*w \tag{28}$$

$$\implies \tilde{y} = U^*U\Lambda V^*VQ\tilde{x} + U^*w. \tag{29}$$

Thus, capacity of the system from (23) reduces to[3]

$$
\begin{aligned}
C &= \log_2 \det \left(I_{n_R} + \frac{1}{\sigma_n^2} Q H_{\text{eq}}^* H_{\text{eq}} \right) \\
&= \log_2 \det \left(I_{n_R} + \frac{1}{\sigma_n^2} Q V^* H^* H V \right) \\
&= \log_2 \det \left(I_{n_R} + \frac{1}{\sigma_n^2} Q \Lambda^2 \right) \text{ bits/s/Hz.}
\end{aligned} \tag{30}
$$

Where H_{eq} is the effective channel seen by the receiver. Equation(27) shows that the channel H can be decomposed into n_S parallel SISO channels as shown in Figure 10
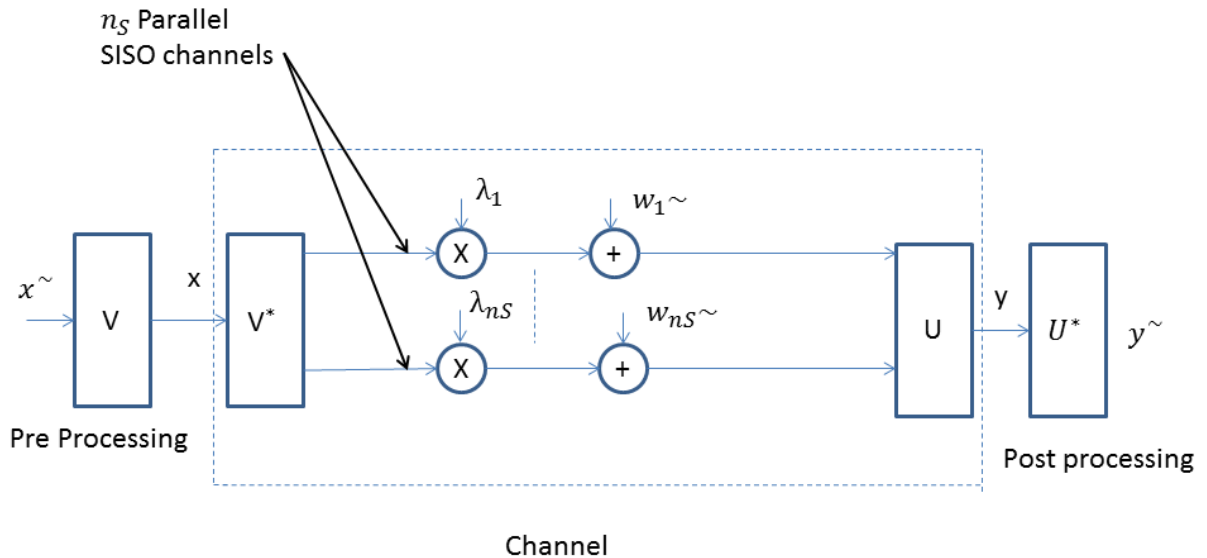

Figure 10: MIMO as n_S parallel SISO channels.

Thus, (29) is

$$\tilde{y}_i = \lambda_i \tilde{x}_i + \tilde{w}_i, \quad i = 1, 2, ..., n_S \tag{31}$$

The capacity of MIMO system, (30) is thus the sum of n_S parallel SISO channel

---

[3]Since we have assumed perfect CSIT for analytic purposes, $H_{\text{eq}} = HV$

capacities [1, page 292-293] given by

$$C = \sum_{i=1}^{n_S} \log_2\left(1 + \frac{P_{s,i}^* \lambda_i^2}{n_S \sigma_n^2}\right) \text{bits/s/Hz}. \tag{32}$$

Where $P_1^*, ..., P_{n_S}^*$ are the water-filling power allocations to each of the transmit antennas:

$$P_{si}^* = \left(\mu - \frac{\sigma_n^2}{\lambda_i^2}\right)^+,$$

where μ is a variable chosen to satisfy the power constraint: $\sum_{i=1} P_{si}^* \leq P_s$ [16, page 37-38]. Each λ_i^2 corresponds to a Eigenmode of the channel. The symbol, $()^+$ is a function that sets negative numbers to zero.

2.5.2 Capacity of a Random MIMO channel

Until now, we have assessed the MIMO capacity for a deterministic channel. In general, however, the channel is randomly varying with time. Which means that channel capacity is also randomly time varying. In other words, the MIMO capacity is given by its time average. This Shannon channel capacity can be achieved only when coding is performed over infinitely long, independent channel matrix realizations.

$$\mathcal{H} \ni \boldsymbol{H_i} \qquad i = 1, ..., \infty$$

Thus, we assume that the random channel is an ergodic process.

Ergodic channel capacity   *The ergodic capacity of a MIMO channel is the ensemble average of the information rate over the distribution of the elements of the channel matrix $\boldsymbol{H}$ is given by* [17] [1]

$$C = \mathcal{E}_{\mathcal{H}}\left[\max_{\text{Tr}(\boldsymbol{Q}=n_T)} \log_2 \det(\boldsymbol{I}_{n_R} + \frac{1}{\sigma_n^2} \boldsymbol{HQH^*})\right] \text{bits/s/Hz}, \tag{33}$$

which is sometimes referred to as ergodic channel capacity. For example, the ergodic channel capacity with and without CSI at the transmitter is given by

$$C = \mathcal{E}_{\mathcal{H}}\left[\log_2 \det(\boldsymbol{I}_{n_R} + \frac{1}{\sigma_n^2} \boldsymbol{Q\Lambda^2})\right] \text{bits/s/Hz} \tag{34}$$

and

$$\tilde{C} = \mathcal{E}_{\mathcal{H}}\left[\log_2 \det(\boldsymbol{I}_{n_T} + \frac{P_s}{\sigma_n^2} \boldsymbol{\Sigma})\right] \text{bits/s/Hz} \tag{35}$$

respectively. From (32)(34), we can appreciate the increase in channel capacity of a MIMO system over a SISO/SIMO/MISO using spatial multiplexing and water-filling concepts.

Outage Capacity :

The ergodic channel capacity is a relevant performance metric in the case of a fast fading channel. Where we maximize the average rate of information flow through the channel in order to achieve ergodic channel(Shannon's) capacity. However, in the case of a slow fading, averaging is not possible over all channel realizations. The transmission rate is a random variable which depends on the quasi static channel not making ergodic capacity a feasible measure. Thus, the objective is to ensure reliable transmission by minimizing the probability that the rate of information flow falls below a target rate $\boldsymbol{R}$ bits/s/Hz. We can achieve reliable communication as long as it satisfies [1, page 187]:

$$\log_2 \det(\boldsymbol{I}_{n_R} + \frac{\boldsymbol{HQH}^*}{\sigma_n^2}) \geq \boldsymbol{R}. \tag{36}$$

If MIMO channel is unable to satisfy the (36) then we are in outage. The outage probability is given by

$$p_{\text{out}}^{\text{mimo}}(\boldsymbol{R}) = \max_{\text{Tr}(\boldsymbol{Q} \leq \text{P}_s)} \mathcal{P}\left(\log_2(1 + ||\boldsymbol{H}||^2 \leq \boldsymbol{R}\right), \tag{37}$$

and the corresponding performance metric for a slow fading MIMO channel is outage capacity.

We also mention to our readers that from here on we set the covariance matrix, $\boldsymbol{Q}$ to $\boldsymbol{I}$ though we consider partial CSIT.

2.5.3 Diversity-Spatial multiplexing trade off

MIMO channel basically offers diversity and spatial multiplexing gain. However, higher spatial multiplexing comes at a price of sacrificing diversity gain and vice-versa. Both gains can be simultaneously obtained, but there is a fundamental trade off. This trade off speaks about the dual benefits of a MIMO communication channel in the high SNR regime.

In a slow fading i.i.d Rayleigh MIMO channel, the objective is to ensure reliable transmission, in other words to achieve *maximum diversity gain*. For a given $n_T \times n_R$ MIMO channel, the maximum diversity gain is found to be $n_T n_R$ (for a fixed rate $\boldsymbol{R}$ [1, page 384]) and the outage probability decays in the form $\frac{1}{SNR^{n_T n_R}}$ [18] in the high SNR regime. On the contrary, we emphasize on maximizing the average rate of information flow using spatial multiplexing in the case of fast fading channel. This gain is provided by the additional degrees of freedom n_S. It has been shown by Foschini [18, 19] that at high SNR, the capacity of the MIMO channel is given by

$$C = n_S \log(SNR) \qquad n_S = \min(n_T, n_R) = \text{rank}(\boldsymbol{H}). \tag{38}$$

When we want to have reliable communication(maximum diversity gain), the target rate($\boldsymbol{R}$) is fixed. At high SNR, the channel capacity in (38) grows dwarfing

R. From this, we observe that there is no effective utilization of degrees of freedom thereby compromising on spatial multiplexing gain. Thus, there is a need for diversity-multiplexing trade off.

[18]A MIMO communication system is said to have achieve diversity gain $d^*(r)$ if the data rate

$$R = r \log \text{SNR}$$

and the outage probability is

$$P_{\text{out}}(R) \approx \text{SNR}^{-\text{d}^*\text{(r)}},$$

taking log and applying limits we get,

$$\lim_{\text{SNR} \to +\infty} \frac{\log p_{\text{out}}(r \log \text{SNR})}{\log \text{SNR}} = -d^*(r). \tag{39}$$

$d^*(.)$ is referred to as diversity multiplexing trade off.

if the multiplexing gain $r \to 0$ then we achieve maximum diversity gain $n_T n_R$, else a maximum multiplexing gain of n_S with no diversity gain. Therefore, optimal trade off was proposed (39) in order to strike a balance between diversity and multiplexing gain.

2.5.4 Environmental factors affecting MIMO capacity

MIMO systems are used to increase the spectral efficiency by using spatial multiplexing. However, with the increase of transmit and receive antennas, the capacity of the system will be severely affected by the environmental factors. In this final section we shall briefly review the factors which affect the performance of MIMO systems. The factors are channel complexity, external interference, and channel stationarity [20].

Channel complexity The channel matrix H plays a vital role in determining the channel capacity. It is a function of richness of scatterers. The spectral efficiency increases with the increase in singular values. For analytic purposes, H can be assumed to have i.i.d Gaussian complex channel gains. But, this kind of matrix may lead to flat singular values distribution [20]. On the other hand, the channel can be ascertained based on diversity order, which gives an insight into the spatial correlation of the channel [21].

Interference A given MIMO system may have to work with several other MIMO systems. As a result, there is bound to be a lot of interference from the other systems, cases such as mutli-user MIMO systems, wifi bands operating in unlicensed bands are some good examples.

Channel Stationarity There are generally two communication scenarios, i.e., one being stationary and the other being mobile. In a stationary environment, though

the channel is considered to be static, in a practical system the channel estimation is limited because the environment changes after certain time duration. Thus, the transmitter will have the knowledge of previous channel estimates which results in a greater error in channel estimation at the transmitter [20], thereby affecting the system capacity.

With the MIMO system model in mind, we move onto our next part of brief literature study on manifolds.

3 Manifolds

In the previous section, we discussed some aspects of MIMO wireless systems. In this section we describe metric spaces, differentiability, notion of tangent vectors, and related aspects of manifolds. Furthermore, we concentrate on specific manifolds that are used for our codebook design laying out the foundation for solving the proposed research problem. An in-depth analysis of manifolds and group theory is beyond the scope of this thesis.

3.1 Metric spaces

3.1.1 Cauchy sequence

For any arbitrary set X, Cauchy sequence is a sequence whose elements in X become arbitrarily close to each other as the sequence progresses. In other words, the infinite sequence $(x_1, x_2, ...)$ of points in X converges to a point $x_m \in X$. The formal definition is stated as [22]:

A sequence $x_1, x_2, ...$ of real numbers is called Cauchy, if for every positive real number δ, there is a positive integer n_0 such that for all natural numbers $m, n > n_0$ $|x_m - x_n| < \delta$.

This notion of convergence can be further extended to $\mathcal{R}^n$ with $n-$tuples of real numbers using the distance function

$$d(\boldsymbol{x}, \boldsymbol{y}) := \sqrt{(\boldsymbol{x} - \boldsymbol{y}).(\boldsymbol{x} - \boldsymbol{y})} \tag{40}$$

3.1.2 Concept of metric spaces

We can generalize the distance function defined in (40) on any set X by analyzing the notion of convergence of the Euclidean distance $d(\boldsymbol{x}, \boldsymbol{y})$. This generalization leads to a metric on set X

Distance metric [23, page 158,159]: A metric on a set X is a map $d : X \times X \to \mathcal{R}$ that satisfies the three conditions

$$d(x, y) = d(y, x) \qquad \text{(symmetry)}$$

$$d(x, y) \geq 0, and = 0 \quad \text{iff} \quad \text{x = y}$$

$$d(x, y) \leq d(x, z) + d(z, y) \qquad \text{triangle inequality}$$

for all $x, y, z \in X$.

Thus, endowed with a metric d, the set X is sometimes referred as metric space denoted by (X, d).

3.1.3   Points, subsets in metric spaces

Let us consider a subset U of the metric space X with a metric d. The ball (Figure11) around a point x of radius δ is formally defined as

$$B_x(\delta) := \{x^{'} \in \mathcal{C} | \quad |x - x^{'}| < \delta\}. \tag{41}$$

Every point in X belongs to one of the *three* categories w.r.t $U \subset X$ mentioned below [24, page 12]:
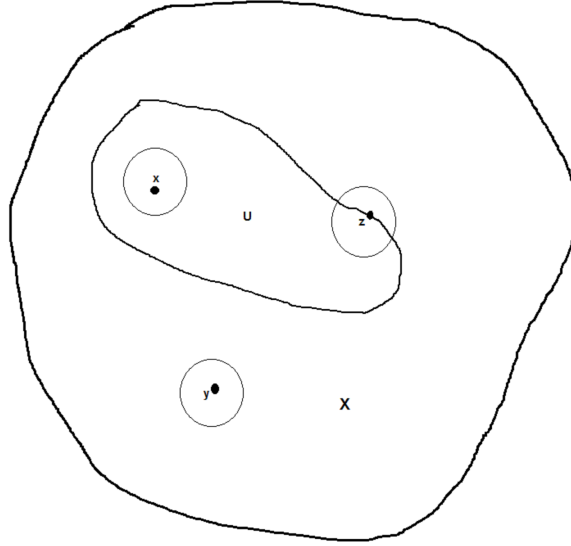
Figure 11: Illustration of an interior, an exterior, and a boundary point.

1) *x is an interior point if there exists $\delta > 0$ such that the ball $B_x(\delta)$ around $x \in X$ has the property that $B_x(\delta) \subset U$.*

2) *y is an exterior point if there exists $\delta > 0$ such that the ball $B_y(\delta)$ has the property that $B_y(\delta) \cap U = \Phi$.*

3) *z is a boundary point of U if every ball $B_z(\delta), \delta > 0$ intersects both A and A^c*

The set of all *interior*, *exterior*, and *boundary* points of U are denoted by Int(U), Ext(U), and Bd(U) respectively. A set U is said to be *open* iff $U = Int(U)$ excluding the boundary points $Bd(U)$. The collection of all open sets of metric space X is called the topology of the space X [24, page 13].

3.2   Differentiable manifold

In order to understand the notion of differentiable manifold, we shall consider a topological space $\mathcal{M}$ to be connected, Hausdorff space and also delineate relevant

concepts . A topological space $\mathcal{M}$ is said to be connected if it cannot be represented as the union of *two* or more disjoint nonempty open subsets, and is said to be a Hausdorff space [25] if given points (x and $y \in \mathcal{M}$) can be separated by disjoint neighborhoods, i.e., there exists a neighborhood U of x and a neighborhood V of y such that U and V are disjoint($U \cap V = \Phi$). See Figure12.
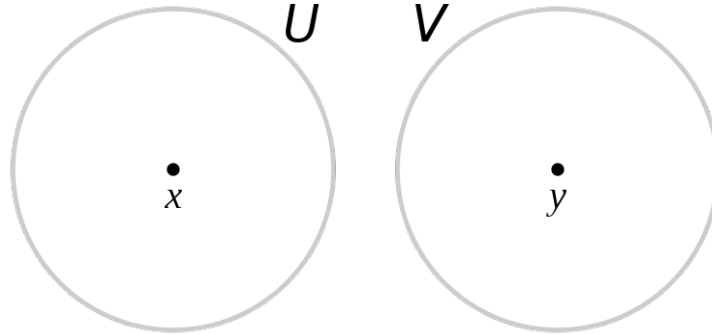
Figure 12: Points x and y separated by neighborhoods U and V respectively.

Definition 1. *A function* f : $X \to Y$ *is a* homeomorphism*(isomorphism in general topology) if and only if i)*f *is a bijective ii)*f *is continuous and iii)*f^-1 *is also continuous* [26] [27, page 449-452] .

3.2.1   Coordinate chart

A coordinate chart on m- dimensional $\mathcal{M}$ is a pair (U, ϕ) consisting of an open subset $U \subset \mathcal{M}$ and a map $\phi : U \to \mathcal{R}^m$ such that $\phi(U)$ is open. The map ϕ is a homeomorphism between U and $\phi(U)$. [28, page 18-20] as illustrated in Figure 13. An atlas of dimension m on $\mathcal{M}$ is a collection of pairs (U_i, ϕ_i) (i ranging in some indexing set I), satisfying the following conditions [24, page 62],

i) The union of all the pairs $\cup_{i \in I} U_i$ constitutes the topological space $\mathcal{M}$.

ii) We have two over lapping coordinate charts such that $U_1 \cap U_2 \neq \Phi$. The overlap function between the coordinate charts is the map $\phi_2 \circ \phi_1^{-1}$ from $\phi_1(U_1 \cap U_2) \to \phi_2(U_1 \cap U_2)$, where both are open subsets $\subset \mathcal{R}^m$ as shown in Figure 14. The second condition is that the map

$$\phi_2 \circ \phi_1^{-1} : \phi_i(U_i \cap U_j) \to \phi_j(U_i \cap U_j)$$

must be a C^∞ map. Where C^∞ is a smooth function, having partial derivatives of all orders. For an atlas, the collection of all the pairs $(U_i, \phi_i)_{i \in I}$ is referred to as a differential structure on $\mathcal{M}$. Thus, the topological space $\mathcal{M}$ is said to be a *differentiable manifold* or m-manifold [24, page 62]. One of the prominent examples of a n-dimensional *differentiable manifold* is subset $\mathcal{S}^n := \{\vec{x} \in \mathcal{R}^{n+1} : ||\vec{x}|| = 1\}$.

Figure 13: A local coordinate chart

Figure 14: Overlap function of coordinate charts
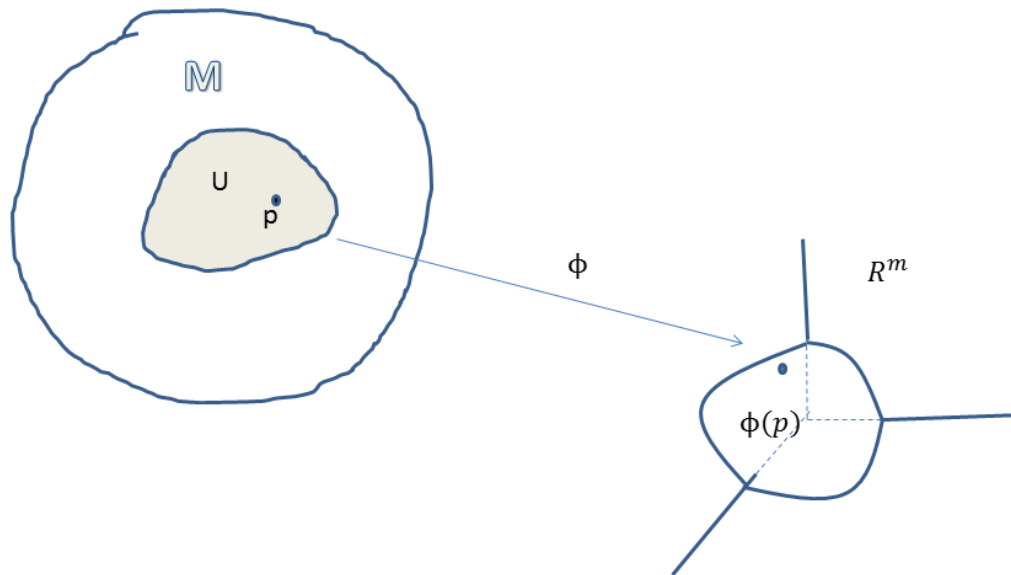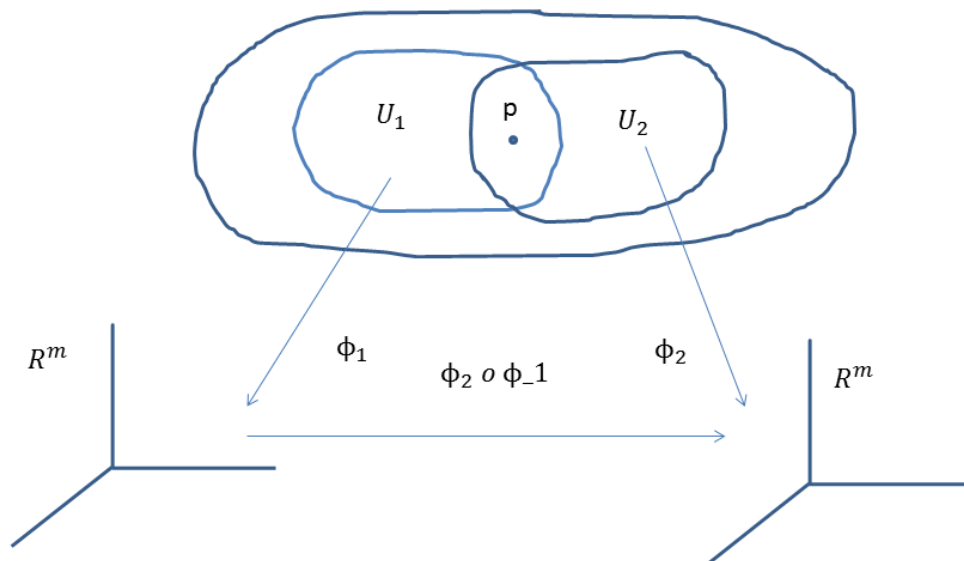
3.3   Tangent Space

Tangent spaces is one of the most important, useful ideas of differential geometry. To a certain extent, we can regard the tangent space as the linearization of the manifold at a point.

3.3.1 The notion of a Tangent vector

The geometrical representation of a tangent vector $\vec{v}$ to a curve on a manifold $\mathcal{S}^n$ embedded in a $\mathcal{R}^{n+1}$ is shown in Figure 15 [24, page 73].
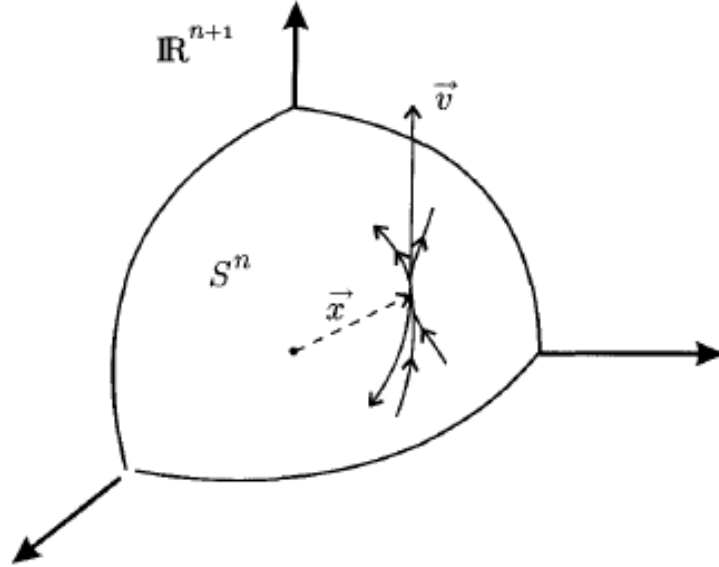
Figure 15: A tangent vector $\vec{v}$ at point $\vec{x} \in \mathcal{S}^n$

In Figure 15, the tangent vector $\vec{v}$ is the tangent to the curves at point $\vec{x}$. Since these curves lie on the manifold, we can say that $\vec{v}$ is a tangent vector to the manifold($\mathcal{S}^n$) itself. Thereby generalizing the *tangent to a curve* to the *tangent to the manifold* [28, page 53]. However, a closer observation of Figure 15 reveals that there are two curves(σ_1,σ_2) having the same tangent vector. Thus, the notion of tangent vector represents *equivalent class* of curves, i.e. $\vec{v} = [\sigma]$.

The pictorial representation of *two* tangent vectors($\vec{v_1},\vec{v_2}$) for two non-equivalent curves (σ_1,σ_2) respectively, at a given point $(p \in U \subset \mathcal{M})$ is illustrated in Figure (16). The collection of all tangent vectors at p constitutes the tangent space $\mathcal{T}_p\mathcal{M}$ to $\mathcal{M}$ at p. The tangent space can be regarded as a linear subspace of the vector space $\mathcal{R}^{n+1}$, and the tangent bundle $\mathcal{T}\mathcal{M}$ is defined as $\mathcal{T}\mathcal{M} = \cup_{p\in\mathcal{M}}\mathcal{T}_p\mathcal{M}$ [28, page 57].

3.3.2 Alternate approach to the notion of tangent vector

Motivated by the notion of *directional directive*, the tangent vector v can be defined [24, page 79] as

$$\vec{v}(f) = \frac{df(\sigma(t))}{dt}; \quad t := 0$$

The tangent vector acts as a differential operator on the differentiable manifold $\mathcal{M}$. The manifold $\mathcal{M}$ can be regarded as a ring over $\mathcal{R}$ [24, page 79,80], tangent vector as a derivation map from this ring to $\mathcal{R}$. The set of all derivations at $p \in \mathcal{M}$
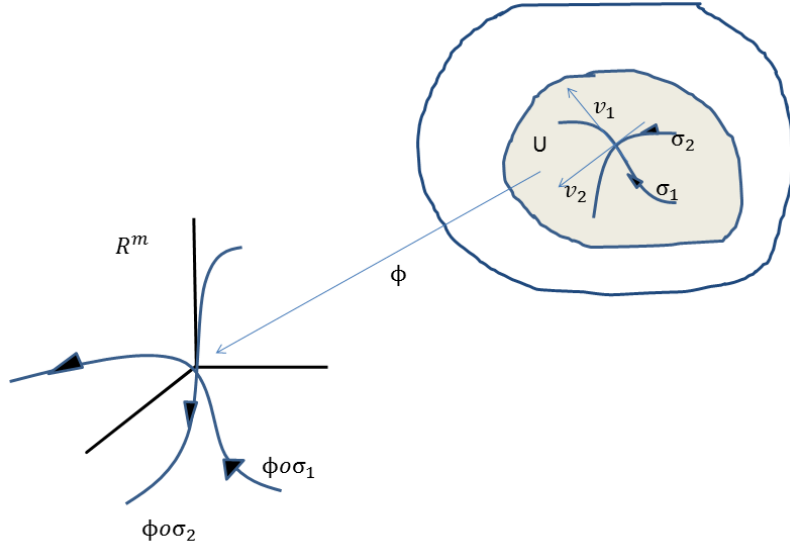
Figure 16: tangent space, collection of all vectors at point p

is denoted as $D_p\mathcal{M}$ [24, page 79,80]. This alternate approach is intrinsic as opposed to the geometrical representation of tangent vector because latter doesn't involve embedding the manifold in any Euclidean space.

3.4 Riemannian Manifold

A *Riemannian manifold*$(\mathcal{M},g)$ is a *differentiable manifold* equipped with a *Riemannian metric,g*. The *Riemannian metric*

$$g_p : \mathcal{T}_p\mathcal{M} \times \mathcal{T}_p\mathcal{M} \to \mathcal{R}, \qquad p \in \mathcal{M}$$

is the collection of all Riemannian inner products, $< .,. >_p$, defined in the tangent space $\mathcal{T}_p\mathcal{M}$ for every point $p \in \mathcal{M}$ [29]. A differentiable manifold having a local coordinate system $p = (p^1, ..., p^n)$ induces a basis $\frac{\partial}{\partial p} = (\frac{\partial}{\partial p^1}, ..., \frac{\partial}{\partial p^n})$ on the tangent space $\mathcal{T}_p\mathcal{M}$. Hence, we have the dot product of the tangent vector to the coordinate curves : $g_{ij}(p) :=< \frac{\partial}{\partial p^i}, \frac{\partial}{\partial p^j} >$. The collection of all the dot products can be represented as a *symmetric positive* matrix:$G[p] = g_{ij}(p)$ [30]. Thus, we have the dot product between two tangent vectors $< v, w >_p = v^T G[p] w$ (From here on we shall represent $\vec{v}$ as v). This matrix $G[p]$ is called the *local representation* of *Riemannian metric* in the tangent space [30].

Geodesic of a Manifold For a differentiable manifold $\mathcal{M}$ endowed with a Riemannian metric g, the minimum length of a curve joining the points p, $q \in \mathcal{M}$ is

defined [30] as

$$d(p, q) = \min_{\gamma} \int_a^b ||\dot{\gamma}(t)|| dt = \int_a^b \left(< \dot{\gamma}(t), \dot{\gamma}(t) >_{\gamma(t)} \right)^{\frac{1}{2}} dt \qquad (42)$$

where the *infinum* is over all piece-wise differentiable curves $t \to \gamma(t)$ in $\mathcal{M}$ that pass through the point p and q, which is referred to as the *geodesic*.

For every $p \in \mathcal{M}$ *and every* $v \in \mathcal{T}_p\mathcal{M}$, *there is a unique geodesic on the manifold denoted as* γ_v, *such that* $\gamma(0) = p$ *and its corresponding mapping on the tangent space is* $\dot{\gamma}(0) = v$, *and the domain of* γ *is the largest possible with* γ_v *as the* maximal geodesic *[31]*. The manifold is said to be *geodesically complete* if the manifold has no boundary and no singular point.

Exponential map   There are many fundamental differences between the classical *Euclidean* geometry and the *Riemannian* geometry due to the global topology of the manifold. However, locally Riemannian geometry is similar to Euclidean geometry in many ways. Thus, we introduce the notion of *exponential map*. The whole idea behind the exponential map is to locally express a Riemannian manifold($\mathcal{M}$) at a point p in terms of the tangent space $\mathcal{T}_p\mathcal{M}$ [31], the tangent vectors explained in terms of their corresponding geodesics. The formal definition of an exponential map is [31]:

Let $(\mathcal{M},g)$ be a Riemannian manifold. For every $p \in \mathcal{M}$, let $\mathcal{D}(p)$ be the open subset of $\mathcal{T}_p\mathcal{M}$ given by

$$\mathcal{D}(p) := \{v \in \mathcal{T}_p\mathcal{M} | \gamma_v(1) \quad \text{is defined}\},$$

with γ_v as the unique maximal geodesic, and initial conditions $\gamma_v(0) = p$ and $\dot{\gamma}_v(0) = v$. The *exponential map* is the map, $\exp_p : \mathcal{D}(p) \to \mathcal{M}$, given by

$$\exp_p(v) = \gamma_v(1).$$

3.4.1   Grassmann Manifold

Let n,p be two positive integers such that $n > p$. The *Grassmann manifold* represents the p-dimensional *linear* subspaces of $\mathcal{R}^n$ often denoted as $\mathcal{G}_{n,p}$, which is a special case of Riemannian manifold.

An element $\mathcal{Y}$ in $\mathcal{G}_{n,p}$ can be specified by a basis, i.e. a set of p *orthonormal* vectors $\boldsymbol{y}_1, ..., \boldsymbol{y}_p$ such that $\mathcal{Y}$ is the set of all their linear combinations . When these orthonormal vectors are ordered as the columns of a matrix $\boldsymbol{Y} \in \mathcal{C}^{n \times p}$ [32], then $\boldsymbol{Y}$ is said to *span* $\mathcal{Y}$ and $\mathcal{Y}$ is said to be the *column space* of $\boldsymbol{Y}$ [32] [33]. The span of matrix $\boldsymbol{Y}$ is an element on $\mathcal{G}_{n,p}$ iff $\boldsymbol{Y}$ has only orthonormal vectors.

$$\mathcal{V}_{n,p} := \{\boldsymbol{Y} \in \mathcal{C}^{n \times p} : \boldsymbol{Y}\boldsymbol{Y}^* = \boldsymbol{I}\}$$

An element $\mathcal{Y}$ of $\mathcal{G}_{n,p}$ may present the image of many different column spaces, $\boldsymbol{Y}_i$ for $1 \leq i < \infty$ spanning the same subspace. Thus, for a given matrix $\boldsymbol{Y} \in \mathcal{V}_{n,p}$, the set of matrices which have the same span as $\boldsymbol{Y}$ is given by [33]:

$$Y\mathcal{U}_p := \{YM : M \in \mathcal{U}_p\} \tag{43}$$

where $\mathcal{U}_p$ represents the set of $p \times p$ unitary matrices. We identify $\mathcal{G}_{n,p}$ as the *quotient space* [34, page 63] [33] of

$$\mathcal{V}_{n,p}/\mathcal{U}_p. \tag{44}$$

The complex Stiefel manifold in this thesis is represented as the quotient space $\mathcal{U}_n/\mathcal{U}_{n-p}$. Thus, (44) is modified to

$$\mathcal{U}_n/(\mathcal{U}_{n-p} \times \mathcal{U}_p), \tag{45}$$

where $\mathcal{U}_n$ represents the set of n-by-n unitary matrices.

Distance metric The concept of Euclidean or chordal distance in $\mathcal{G}_{n,p}$ can be defined in terms of *principal* angles between the elements $\mathcal{Y}_1, \mathcal{Y}_2 \in \mathcal{G}_{n,p}$ [35] The SVD of $Y_1 Y_2^*$ is given by $U(\cos\Theta)V$, where $\cos\Theta = diag(\cos\theta_1, ..., \cos\theta_p)$ and $\{\theta_i\}_{i=1}^p$ are the principal angles between the sub-spaces spanned by the elements $\mathcal{Y}_1, \mathcal{Y}_2$ [36]. The chordal distance metric on $\mathcal{G}_{n,p}$ is given by [36]

$$d(Y_1, Y_2) = \frac{1}{\sqrt{2}}||Y_1 Y_1^* - Y_2 Y_2^*||_2 = ||\sin\Theta||_2 \tag{46}$$

3.4.2 Permutation Invariant Flag Manifold

A complex *flag* manifold is a *homogeneous space* whose points also referred to as *flags*, represents finite dimensional vector space **V** with $\dim(V)_i = n_i$ over a field **F** in an ordered sequences of subspaces. It is mathematically defined as

$$\{0\} = \mathbf{V}_o \subset \mathbf{V}_1 \subset \mathbf{V}_2..... \subset \mathbf{V}_n.$$

We consider a unitary group $\mathcal{U}_n$ consisting of $n \times n$ unitary matrices. Some of these unitary matrices in $\mathcal{U}_n$ may be equivalent. We define two equivalence relations for a unitary matrix $U \in \mathcal{U}_n$ such that $U \sim U\Theta$ and $U \sim UP$, where Θ and P are arbitrary rotation and permutation matrices respectively. In addition, we also define $\mathcal{X}_n = \{X : X = P\Theta \text{ or } \Theta P\}$ for $\Theta \in \Theta$ and $P \in \mathcal{P}$, where Θ and $\mathcal{P}$ are sets of rotation and permutation matrices respectively [37].

We can extract a representative from each equivalence class by considering the quotient space defined as [37]

$$\mathcal{F}_{n,n} = \mathcal{U}_n/\mathcal{X}_n, \tag{47}$$

this quotient space consists of unitary points which are non-equivalent.

Distance metric For a given *unitary group* $\mathcal{U}_{n \times n}$ is a *Lie group* [38](see Appendix). $\mathcal{X}_{n \times n}$ forms a *closed Subgroup* of $\mathcal{U}_{n \times n}$ under matrix multiplication [37].Since any *unitary matrix* is an isometry with respect to the norm, we consider the *quotient*

space $\mathcal{F}_{n\times n}$ of $\mathcal{U}_{n\times n}/\mathcal{X}_{n\times n}$ is a *homogeneous* space which are in essence *Riemannian* manifolds [37]. The Euclidean distance defined in this flag manifold[4]is given by

$$d(\boldsymbol{U}, \boldsymbol{V}) = \sqrt{n - \max_{\pi(.)} \sum_{m=1}^{n} |\boldsymbol{u}_{\pi(m)}^{*} \boldsymbol{v}_m|^2} = \sqrt{n - \sum_{m=1}^{n} |\boldsymbol{u}_{\tilde{\pi}(m)^{*}} \boldsymbol{v}_m|^2}, \qquad (48)$$

where $\boldsymbol{U}, \boldsymbol{V}$ are unitary matrices belonging to the quotient space, $\tilde{\pi}(.)$ is the maximizing permutation function in (48) or in other words $\boldsymbol{U}$ is permuted to $\boldsymbol{U}'$ w.r.t $\boldsymbol{V}$ such that the distance function is minimized. This distance generalizes the per column chordal distance defined in the Grassmann manifold, since it can be viewed as sum of n chordal distances for the permuted columns of the precoding matrix [37].

---

[4]Flag manifold is a very general term, our permutation invariant flag manifold is a specific case of flag manifold, however, from now on we just address as flag manifold for the sake of simplicity.

4 Precoding

In conventional single stream beamforming, the same signal is emitted from each of the transmit antennas with appropriate weighting such that the signal power is maximized at the receiver output. When the receiver has multiple antennas, single stream beamforming cannot simultaneously maximize the signal level at all of the receive antennas. Thus, in order to maximize the throughput in multiple receive antenna systems, multi-stream beamforming or commonly referred to as precoding is required.

Precoding involves the use of certain predetermined matrices, codewords known to transmit and receive antennas. A codebook is a set containing these distinct, non equivalent codewords. MIMO systems employing precoding are commonly known as limited feedback systems as shown in Figure 17. This section initially gives a brief description of limited feedback MIMO systems. To design these codewords, vector quantization concepts and algorithm are utilized to quantize Grassmann and flag manifolds, which are explained in the remaining parts of the section.

4.1 Limited Feedback System

When CSI is perfectly available at the transmitter and receiver, singular value decomposition (SVD) precoding is known to achieve the MIMO channel capacity as given in (30). In this approach, the channel matrix is diagonalized by taking an SVD and removing the two unitary matrices through pre- and post-multiplication at the transmitter and receiver, respectively. Then, one data stream per singular value can be transmitted (with appropriate power loading) without creating any interference whatsoever, which is mathematically explained in(27)

Many times perfect CSI cannot be made available to the transmitter in a constantly changing wireless systems, especially for FDD systems, where downlink and uplink channels are of different frequency bands separated by a guard band.Thus they are not reciprocal and as a result there are many imperfections such as channel estimation errors, feedback delay, and also limited feedback bandwidth. Certain CSI imperfections such as feedback delay and estimation errors, can be captured by a statistical channel mean information model [39]. Another important CSI imperfection is the bandwidth constraint over the feedback link, which conveys to the transmitter only finite bits about the nature of the channel. For such cases, the transmitter and the receiver need to maintain a predetermined codebook, i.e., a finite collection of precoding matrices commonly referred to as codewords. For each received codeword index, the transmitter chooses the corresponding precoding matrix for data transmission [39].

4.1.1 Limited Feedback MIMO system model

MIMO system model with finite rate feedback is shown in Figure 17, where M is the precoding matrix, Z is the equalizer which is a linear receiver in our case. The stream $\tilde{x}$ is processed, split into several sub-streams, pre-multiplied with codeword

and transmitted. The received signal, subjected to channel conditions and thermal noise of the receivers, post multiplied at the receiver is given by

$$\tilde{\boldsymbol{y}} = \boldsymbol{ZHM}\tilde{\boldsymbol{x}} + \boldsymbol{Zw}, \tag{49}$$

where $\tilde{\boldsymbol{x}} = [\tilde{x}_1, \tilde{x}_2, ..., \tilde{x}_{n_T}]$, $\tilde{\boldsymbol{y}} = [\tilde{y}_1, \tilde{y}_2, ..., \tilde{y}_{n_R}]$.
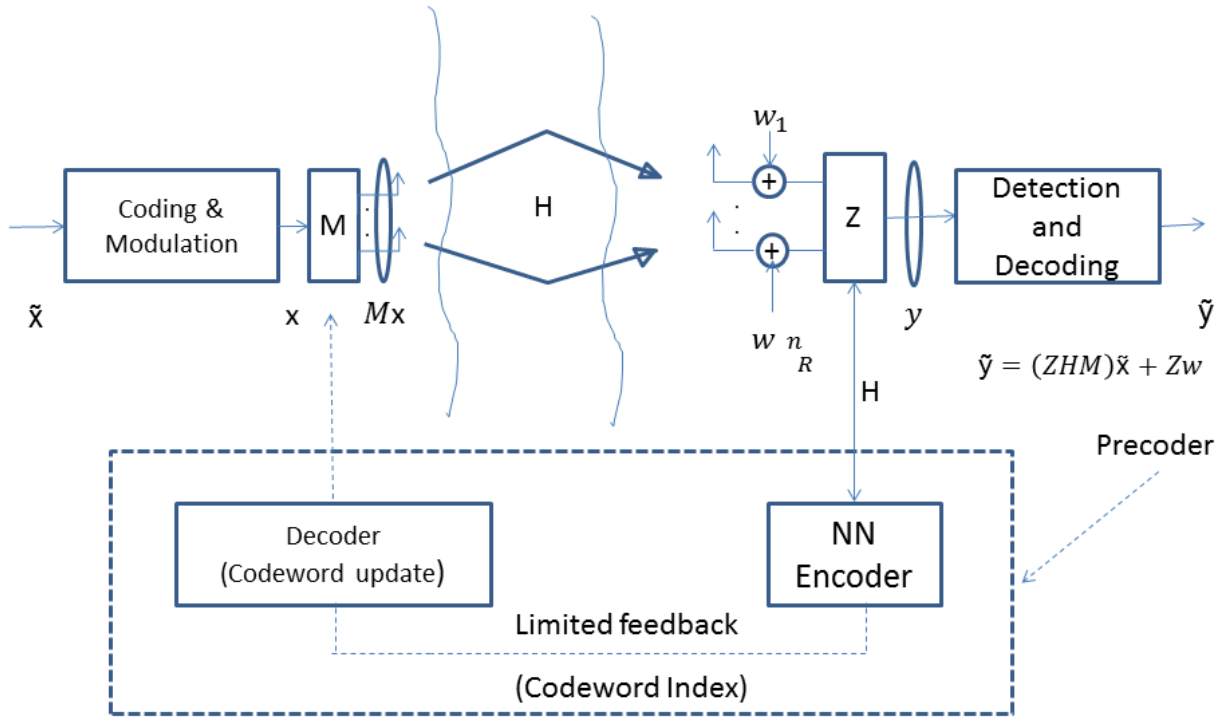
Figure 17: MIMO system model with Precoder.

However, precoding can have an affect on the throughput only when water filling concept is used at the transmitter, else with the complete channel knowledge available at the receiver, we can achieve the same capacity by inverting the channel matrix, recover the symbols as shown in (49) along the Eigen directions.

4.2 Vector Quantization

Roughly speaking, vector quantization(VQ) can be viewed as a form of pattern recognition in which the input pattern is *approximated* to an already known template. However, we discuss VQ in detail to gain an actual understanding of the *generalized Lloyd algorithm.* The structure and basic principles for vector quantization can be generalized to matrix quantization as well [36].

A *vector quantizer* $\mathcal{Q}$ of dimension n and size N is a mapping from a vector in n dimensional complex Euclidean space to a finite set $\boldsymbol{C}$ containing N output vectors referred to as *code words*. It is formally defined as $\mathcal{Q}(\boldsymbol{y}), \mathcal{Q} : \mathcal{C}^n \to \mathcal{C}^n, \boldsymbol{y} \in \mathcal{C}^n$. This

can be extended to a matrix quantizer [36] $\mathcal{Q}(\boldsymbol{Y}), \mathcal{Q} : \mathcal{C}^{n \times p} \to \mathcal{C}^{n \times p}, \boldsymbol{Y} \in \mathcal{C}^{n \times p}, p \leq n$. In the following thesis we have a unitary constraint on $\boldsymbol{Y}$, $\boldsymbol{Y}^* \boldsymbol{Y} = \boldsymbol{I}$, where $\boldsymbol{I}$ is the identity matrix. The set $\boldsymbol{C} := (\boldsymbol{Y'}_1, ..., \boldsymbol{Y'}_N)$ is called as *codebook* comprising of codewords $\boldsymbol{Y'}_i \in \mathcal{C}^{n \times p}$, where $1 \leq i \leq N$. These types of codebooks are generally designed off-line, are known to the receiver in advance. Each codeword induces a partition in $\mathcal{C}^{n \times p}$, denoted as $\boldsymbol{S}_i$, also known as a *Voronoi cell*. This i^{th} cell is defined as [40]

$$\boldsymbol{S}_i = \{\boldsymbol{Y} \in \mathcal{C}^{n \times p} : \mathcal{Q}(\boldsymbol{Y}) = \boldsymbol{Y'}_i\},$$

where the union of all cells $\boldsymbol{S}_i$ is the complex Euclidean space, $\mathcal{C}^{n \times p} := \bigcup_i \boldsymbol{S}_i$ and $\boldsymbol{S}_i \bigcap \boldsymbol{S}_j = \Phi$, $i \neq j$ [40].

The matrix quantizer(MQ), $\mathcal{Q}$ is inherently dependent on *two* conditions: $\boldsymbol{Y'_i}$ and it's corresponding cell $\boldsymbol{S}_i$. Thus, we can represent the quantizer using a *decoder* and *encoder*. The receiver performs the encoding task by mapping a random point $\boldsymbol{Y} \in \boldsymbol{S}_i$ to an index set $\mathcal{I}$; $\mathcal{I} := 1, 2, ..., N$ and then feedbacks this index set to the transmitter, which performs the decoding task. Upon receiving the index set, the transmitter will map it back to $\boldsymbol{Y'_i} \in \boldsymbol{S}_i$. The entire matrix quantization process is mathematically represented as [40]

$$\text{encoder} := \quad \boldsymbol{Y} \in \boldsymbol{S}_\text{i} \to \mathcal{I} \qquad \text{decoder} := \mathcal{I} \to \boldsymbol{Y'_i} \in \boldsymbol{S}_\text{i}, \qquad (50)$$

It can be seen in Figure 18 that MQ is a cascading of encoder and decoder, implying that receiver and transmitter collectively performs the quantization technique.
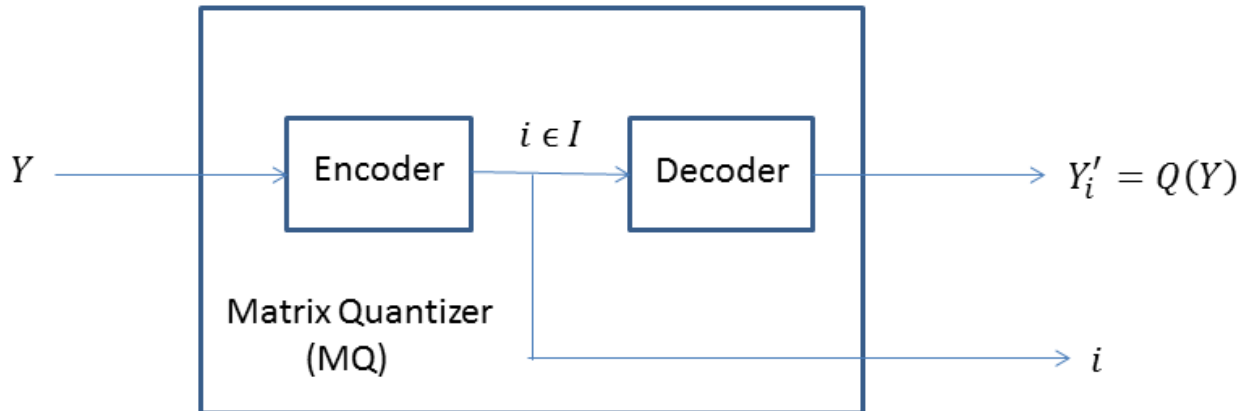
Figure 18: Quantization comprising of encoder and decoder.

4.2.1 Structure of Matrix Quantizer

The encoder's task is to examine each input point $\boldsymbol{Y}$ and identify in which partition cell $\boldsymbol{S}_i$ it lies. The matrix encoder just identifies the *index* of that partition cell which contains $\boldsymbol{Y}$ and the decoder associates the index with the *codeword* representing that partition cell. We model the operation of the encoder described in Figure 19, where the *selector function* $\boldsymbol{\alpha_i}(\boldsymbol{Y})$ is given by [41, page 317]
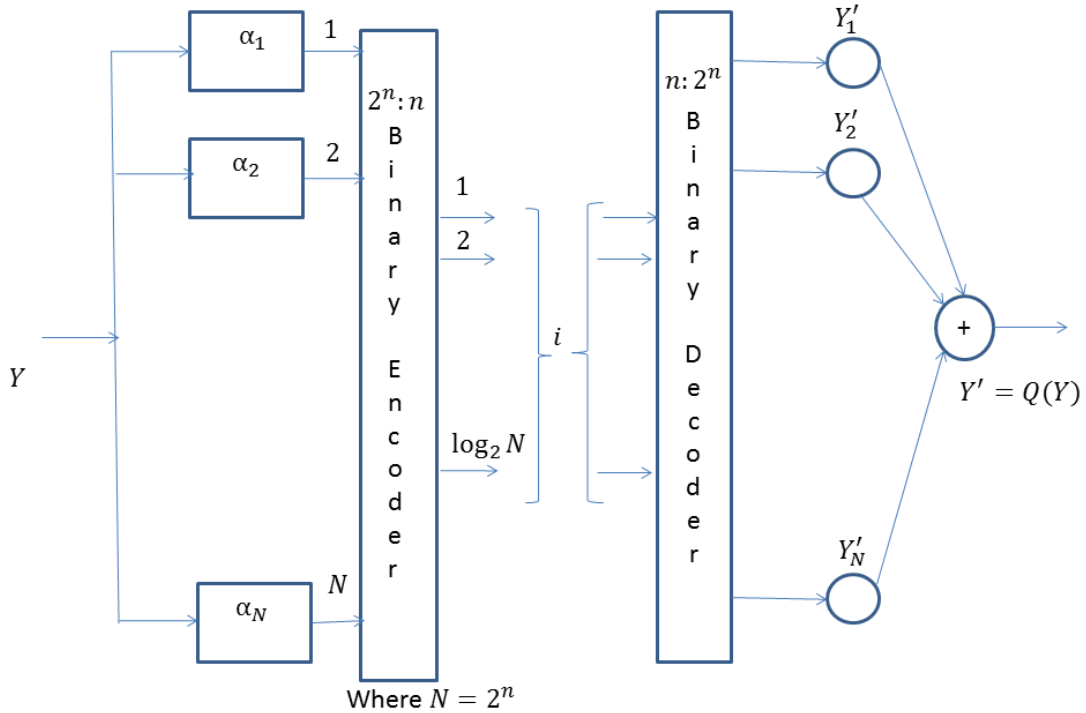
Figure 19: Structural decomposition of the Quantizer.

$$\boldsymbol{\alpha_i}(\boldsymbol{Y}) = \left\{ \begin{array}{ll} 1 & \text{if } \boldsymbol{Y} \in \boldsymbol{S}_i; \\ 0 & \text{otherwise,} \end{array} \right\}$$

We can express the reproduction point, $\boldsymbol{Y'}$ which represents a linear combination of the observable random variables $\boldsymbol{\alpha_i}$

$$\boldsymbol{Y'}_i = \mathcal{Q}(\boldsymbol{Y}) = \sum_{j=1}^{N} \boldsymbol{Y}_j \boldsymbol{\alpha_j}(\boldsymbol{Y})$$

Distortion as a Performance Measure The process of quantization always comes at a price, since approximating a point $\boldsymbol{Y}$ to $\boldsymbol{Y'}$ results in a small error. This error is measured in terms of average distortion(cost) $d_{\text{avgdist}} := \mathcal{E}\{d^2(\boldsymbol{Y}, \boldsymbol{Y'})\}$ which directly gives the accuracy of matrix quantizer. In our thesis, the performance of the

MQ is inversely proportional to the average distortion. When a sequence of random points $\mathcal{Y}$ is *stationary* and *ergodic*, then we can approximate the average distortion D as

$$d_{\text{avgdist}} = \lim_{M \to +\infty} \frac{1}{M} \sum_{k=1}^{M} d^2(\boldsymbol{Y_k}, \boldsymbol{Y'}). \tag{51}$$

The choice of a distortion measure should be such that, it should be evaluated in real finite time enabling the receiver to get the appropriate index from the index set. The distortion measure should be amenable to allow analysis and designing of the codebook. One of the most common and widely used distortion measure between the $\boldsymbol{Y}$ and $\boldsymbol{Y'}$ is the *Euclidean* distance between the two points defined as:

$$d(\boldsymbol{Y}, \boldsymbol{Y'}) = ||\boldsymbol{Y} - \boldsymbol{Y'}||_2 \tag{52}$$

The average distortion in (51) becomes

$$d_{\text{avgdist}} = \mathcal{E}\{d^2(\boldsymbol{Y} - \boldsymbol{Y'})\} = \lim_{M \to +\infty} \frac{1}{M} \sum_{k=1}^{M} \sum_{j=1}^{p} \sum_{i=1}^{n} d^2(y_{k,i,j}, y'_{i,j}) \tag{53}$$

where $d(y_{k,i,j}, y'_{i,j})$ is the distortion arising due to quantization in *one* dimension.

Nearest Neighbor Quantizers   There are umpteen number of quantizers available, the quantizer considered here is popularly known as *Voronoi* or *nearest neighbor(NN)* quantizer. In our scenario, the classification problem considered consists of a finite set of training samples $\mathcal{Y} = \{\boldsymbol{Y_1}, ..., \boldsymbol{Y_L}\}$, where the training samples, $L >> M$. A subset of $\mathcal{Y}$, $\boldsymbol{Y_k}$ $1 \le k \le M$ belongs to a particular cell $\boldsymbol{S_i} \in \mathcal{C}^{n \times p}$, and this cell is represented by a *codeword* $\boldsymbol{Y'}_i$. We approximate $\boldsymbol{Y_k}$ to $\boldsymbol{Y'}_i$ based on the distortion measure. By imbibing NN quantizer we redefine the partition cell as

$$\boldsymbol{S_i} = \{\boldsymbol{Y_k} : d(\boldsymbol{Y_k}, \boldsymbol{Y'}_i) \le d(\boldsymbol{Y_k}, \boldsymbol{Y'}_j) \quad all \quad j \in \mathcal{I}\}. \tag{54}$$

In other words, the cell $\boldsymbol{S_i}$ have those points with least distortion when approximated to codeword $\boldsymbol{Y'}_i$ than any other codeword. The encoding algorithm of a NN encoder can be described as [41, page 328]

Table 1: Nearest Neighbor Encoding Rule

STEP1.	Initially set $d_{\text{avgdist}} = d_0$, j=1, i=1
STEP2.	Compute $D_j = d^2(\boldsymbol{Y}, \boldsymbol{Y'}_j)$
STEP3.	If $D_j < d_{\text{avgdist}}$, set $D_j \to d_{\text{avgdist}}$. Set $j \to i$.
STEP4.	If $j < N$, set $j + 1 \to j$ and goto step 2.
STEP5.	Stop. set final index as i.

The resulting index i, encoder output is fedback to the transmitter to complete the quantization process, initially d_{avgdist} is set to a very high value d_0. Based on

the algorithm in Table 1, we describe the encoding operation as

$$\text{en}(\boldsymbol{Y}) = c(\boldsymbol{Y}, \boldsymbol{C}),$$

where the functional operation given by $c(.,.)$ depends only on the distortion measure [41, page 328]. The following Figure 20 illustrates the form of NN encoder
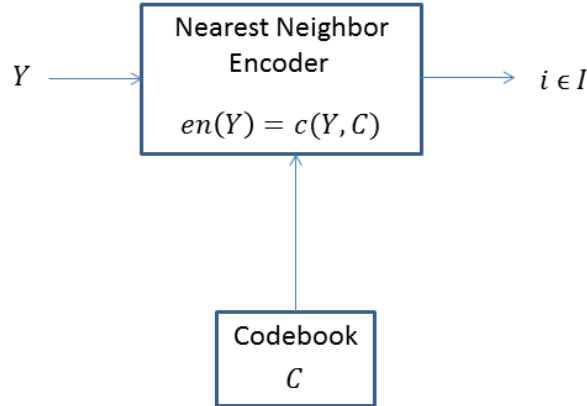

Figure 20: Nearest Neighbor Encoder with a predetermined codebook.

used at the receiver terminal. The primary advantage of NN quantizer is that it does not depend on the geometrical description of cells. But however, the downsides are that the encoding algorithm is computationally intensive and complexity increases with the rise in flow of the information rate.

4.2.2   Optimality Conditions for Quantization

The main objective of a qauntizer is to assign a optimal codebook to the decoder and a corresponding *partition* rule to the encoder such that the entire quantization process minimizes the distrotion measure. Thus, the optimality conditions discussed subsequently provides an optimal codebook for a given partition rule and an optimal partion rule for a given codebook. We first consider the optimization of encoder for a given codebook. Later, we consider decoder optimization for a fixed encoder.

Nearest Neighbor Rule   For a given codebook $\mathcal{C}$ at the decoder, the optimal partition cell is given by (54), i.e., $\boldsymbol{S}_i = \{\boldsymbol{Y}_k : d(\boldsymbol{Y}_k, \boldsymbol{Y}'_i) \leq d(\boldsymbol{Y}_k, \boldsymbol{Y}'_j) \quad all \quad j \in \mathcal{I}\}$. Thus for a fixed decoder, the encoder is a minimum distortion expressed as

$$d_{\text{dist}(\boldsymbol{Y}, \mathcal{Q})} = \min_{\boldsymbol{Y}'_i \in \mathcal{C}} d^2(\boldsymbol{Y}, \boldsymbol{Y}'_i); i \in \mathcal{I} \tag{55}$$

Thus, the *average minimum* distortion is denoted as

$$d_{\text{avgdist}} = \mathcal{E}\{d^2(\boldsymbol{Y}, \boldsymbol{Y}'_i)\} = \frac{1}{M} \sum_{k=1}^{M} d^2(\boldsymbol{Y}, \boldsymbol{Y}'_i); i \in \mathcal{I} \tag{56}$$

A necessary condition which is assumed is the collection of points equidistant from at least two codewords has a *zero* probability, i.e. [41, page 355],

$$P(\boldsymbol{Y} : d(\boldsymbol{Y}, \boldsymbol{Y'}_i) = d(\boldsymbol{Y}, \boldsymbol{Y'}_j, i \neq j) = 0)$$

We next consider the optimal condition for the decoder, given a fixed *partition rule* at the encoder. This leads to our second criterion.

Centroid Condition   We define the centroid, $cent(\boldsymbol{S}_i)$, of any sub space $\boldsymbol{S}_i \in \mathcal{C}^{n \times p}$ as that point $\boldsymbol{Y'}_i$ which minimizes the distortion between point $\boldsymbol{Y}_k, 1 \leq k \leq M$ in $\boldsymbol{S}_i$ and $\boldsymbol{Y'}_i$. Thus [41, page 355],

$$\boldsymbol{Y'}_i = \text{cent}(\boldsymbol{S}_i) \quad \text{if} \quad \mathcal{E}[\text{d}(\boldsymbol{Y}_k, \boldsymbol{Y'}_i)|\boldsymbol{Y}_k \in \boldsymbol{S}_i] \leq \mathcal{E}[\text{d}(\boldsymbol{Y}_k, \boldsymbol{Y})|\boldsymbol{Y}_k \in \boldsymbol{S}_i]$$

for all $\boldsymbol{Y} \in \mathcal{C}^{n \times p}$. This centroid condition is commonly denoted as

$$\text{cent}(\boldsymbol{S}_i) = \arg \min_{\boldsymbol{Y}} \mathcal{E}[d^2(\boldsymbol{Y}_k, \boldsymbol{Y})] = \arg \min_{\boldsymbol{Y}} \sum_{k=1}^{M} [d^2(\boldsymbol{Y}_k, \boldsymbol{Y})] \tag{57}$$

For a fixed partition$\{\boldsymbol{S}_i; i = 1, ..., N\}$ at the encoder, the codewords are optimal if

$$\boldsymbol{Y'}_i = \text{cent}(\boldsymbol{S}_i).$$

4.3   Grassmannian and Flag Manifold Precoding

Precoding, when the codebook stored at both ends is obtained by quantizing Grassmann manifold is commonly referred to as Grassmann precoding. The main aim of Grassmann precoding is to direct all the power to the n_S sub-streams along their corresponding *eigen directions* of the channel, which can be achieved by the selection of appropriate codeword from the set that minimizes the distance [42]

$$d(\boldsymbol{V}^*, \boldsymbol{Y}'_i) = \arg \min_{j \in \mathcal{I}} d(\boldsymbol{V}^*, \boldsymbol{Y}'_j), \tag{58}$$

where d is the chordal distance defined on the Grassmann manifold.

Flag manifold precoding is in a way similar to Grassmann, but the codebook is designed by quantizing the unitary group. Distances on the Grasmannian manifold is defined with respect to subspaces but in flag manifold, each matrix is a full rank matrix belonging to a unitary group. Thus, all unitary precoders share the same subspace [37]. It is due to this reason Grassmann chordal distance is not applicable, the Euclidean distance used in flag manifold is given in 48 and the the power has to be directed to all n_T eigen directions.

5   Codebook design and analysis

In the first part of this section, we derive semi analytical distortion bounds using numerical methods. We also describe the modified Lloyd used to construct our flag manifold codebooks. In the subsequent parts we evaluate our codebooks obtained via Monte Carlo simulations w.r.t. the bounds. Finally, We compare our proposed codebook with the codebook obtained from exhaustive search technique.

5.1   Distortion Bounds

We derive semi analytical bounds for distortion using ball volume calculations. The normalized volume of a geodesic ball plays a very integral part in the analysis of manifold quantization. A geodesic ball in the manifold can be realized as an image of the exponential map [43]. The distances in this ball $\boldsymbol{B}_P(\delta)$ are measured along their geodesics. We represent (41) alternatively as [44, page 24]

$$B_P(\delta) := \{Q \in \mathcal{M} \quad | \quad d(P,Q) \leq \delta\}, \tag{59}$$

however, the geodesic ball in (59) has a boundary. The normalized volume is the ratio of the volume of the ball to that of the volume of the entire manifold given as[5]

$$\mu\big(B(\delta)\big) = \frac{\text{vol}\big(\text{B}(\delta)\big)}{\text{vol}(\mathcal{M})} \tag{60}$$

 The normalized volume of a geodesic ball in $\mathcal{M}_{n \times n}$ is given by [45]

$$\mu\big(B(\delta)\big) \approx c_n \delta^{n^2-n}, \tag{61}$$

where c_n is calculated as follows.

5.1.1   Volume Estimates

Applying the ln operator in (61) we get

$$\ln[\mu(B(\delta))] = \ln[c_n] + (n^2 - n)\ln[\delta],$$

which is a *linear* equation with $n^2 - n$ as the dimension of the quotient group $\mathcal{F}_{n \times n}$. The maximum value of $\mu(B(\delta))$ is unity, i.e., when the ball volume equals the volume of the manifold, the corresponding *critical* radius is δ_c . Figure 21 shows volume estimates for $n = 2, 3, 4$ by simulations.

From the figure, we can see that normalized volume increases linearly w.r.t. δ until the critical point, where $\text{vol}(\text{B}(\delta)) = \text{vol}(\mathcal{M})$. The radius at this point is denoted as δ_c. The critical radius is numerically found to be $1, 1.2, 1.4$ respectively following an *arithmetic progression* series. Thus, generalized expression for $\delta_c{}^6$ is

---

[5]The center of the ball P is dropped since the calculation of the ball volume is independent of the center chosen.
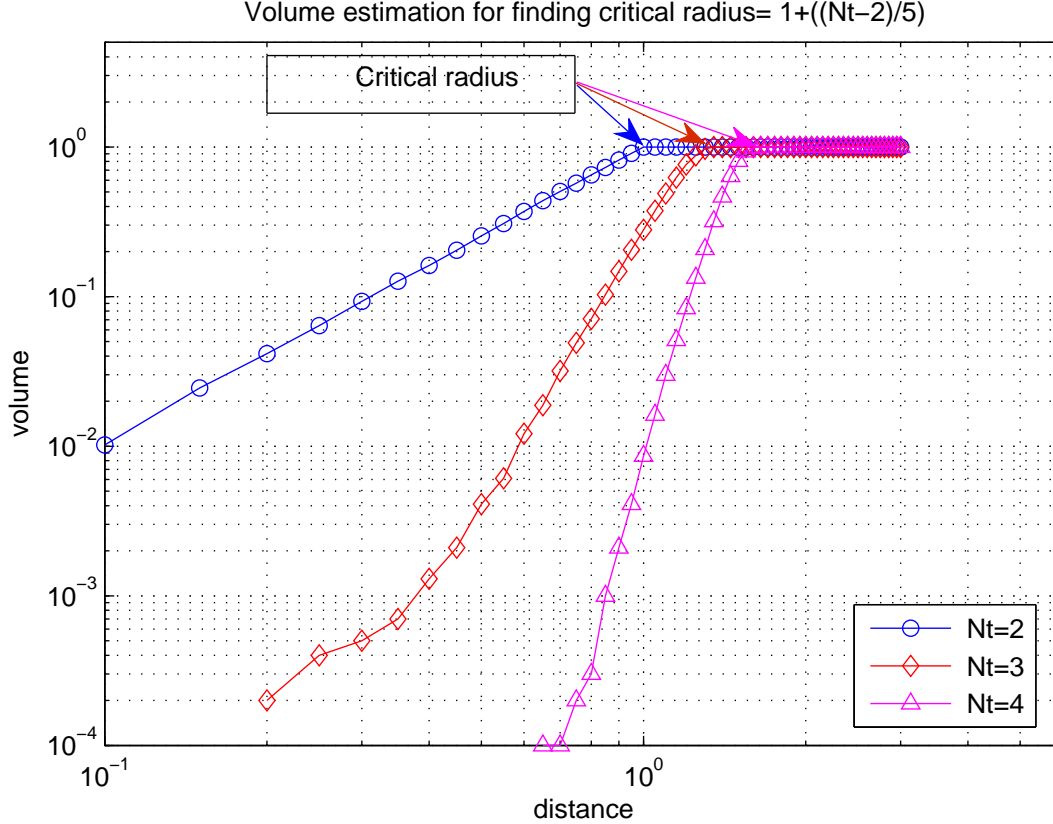
Figure 21: Estimation of δ_c by *trial* and *error* method .

$1 + \frac{N-2}{5}$. By using this expression in (61), we get

$$c_n = \left[1 + \frac{n-2}{5}\right]^{n-n^2}. \tag{62}$$

Figure 22 shows volume estimates for $n = 2, 3, 4, 5, 6$ by simulations. From this figure, we can see that the volume can be well approximated to $c_n\delta^{n^2-n}$, wherein the constant c_n depends only on n as shown in (62).

5.1.2 Analytical Distortion Bounds

For a sufficiently large code size N, the expected value of distortion in using a codeword for quantizing the source points uniformly distributed over a Riemannian manifold can be lower and upper bounded as [45] [44, page 28]

$$\frac{n^2-n}{n^2-n+2}(c_nN)^{\frac{-2}{n^2-n}} \leq d_{\text{avgdist}}(N) \leq \frac{\Gamma(\frac{2}{n^2-n})}{\frac{n^2-n}{2}}(c_nN)^{\frac{-2}{n^2-n}} \tag{63}$$

---

[6]The T_m^{th} term is given by a+(m-1)d, where a is the first term and d is the common difference
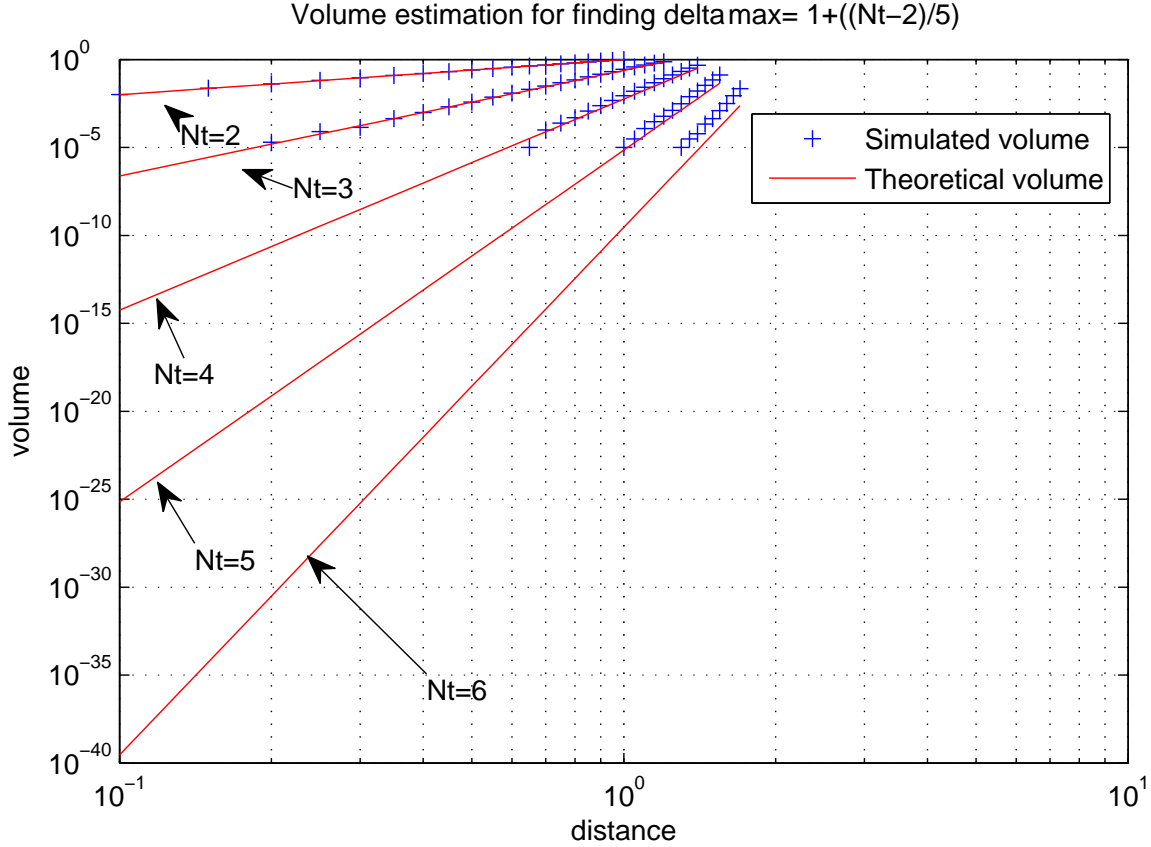
Figure 22: Validation of c_n by approximating simulated volume to $c_n \delta^{n^2-n}$.

Flag Manifold In order to obtain the semi analytical bounds for the source distributed over the flag manifold, we plug in the expression for c_n from (62) in (63) yielding

$$\frac{n^2-n}{n^2-n+2}\left(\frac{n+3}{5}\right)^2 (N)^{\frac{-2}{n^2-n}} \leq d_{\text{avgdist}}(N) \leq \frac{\Gamma(\frac{2}{n^2-n})}{\frac{n^2-n}{2}}\left(\frac{n+3}{5}\right)^2 (N)^{\frac{-2}{n^2-n}} \quad (64)$$

Grassmann Manifold For the source distributed over Grassmann manifold, (63) is modified to

$$\frac{p(n-p)}{(n-p)+1}\left(c_{n,p}N\right)^{-\frac{2}{p(n-p)}} \leq d_{\text{avgdist}} \quad (65)$$

where

$$c_{n,p} = \frac{1}{\Gamma(p(n-p)+1)}\prod_{i=1}^{p}\frac{\Gamma(n-i+1)}{\Gamma(p-i+1)}$$

and N is codebook size, and $n < p$ [46].

5.2 Lloyd Algorithm

One of the best ways of obtaining *optimal codebook* is by iterative codebook improvement algorithm, the most common being Lloyd algorithm which is employed to construct our codebook.

Lloyd algorithm, sometimes known as *K-means* algorithm, is usually used for grouping data points into a given number of clusters. It is an iterative clustering algorithm which starts by partitioning the input space into N regions, $\boldsymbol{S}_1, \boldsymbol{S}_2, ..., \boldsymbol{S}_N$ based on some heuristic. It then calculates the centroid(codeword), $\boldsymbol{Y'}_i$ by averaging the dimensions in Euclidean space and this process is repeated until some criterion is met, in our case it is the distortion rate function [4] [47]. The two necessary conditions required for partitioning are the nearest neighbor condition and the centroid condition.

5.2.1 Algorithm Description

We discuss in detail on the steps involved in quantizing, and constructing codebooks on Grassmann and flag manifolds respectively.

Initiation and training set generation   Set k=0. Generate some random training set $\mathcal{Y} = \{\boldsymbol{Y}_1, ..., \boldsymbol{Y}_L\}$ with uniform distribution on n dimensional space, also choose a set of codewords as the initial codebook $\boldsymbol{Y'}_i(0), 1 \leq i \leq N$, and initialize the mean quantization error(MQE) to $d_{\mathrm{avgdist}}(-1) = +\infty$ as the overall distortion.

Cluster classification   Classify the set of training vectors $\boldsymbol{Y}_l$ into the cluster $\boldsymbol{S}_i$ to associate with the codeword $\boldsymbol{Y'}_i(k)$ by the nearest neighbor condition. For $\forall \boldsymbol{Y}_l \in \mathcal{Y}$, $\boldsymbol{Y}_l \in \boldsymbol{S}_i(k)$, if

$$d(\boldsymbol{Y}_l, \boldsymbol{Y'}_i(k)) < d(\boldsymbol{Y}_l, \boldsymbol{Y'}_j(k)), \quad j \neq i, \quad 1 \leq j \leq N, 1 \leq i \leq N$$

Cluster classification on Grassman manifold uses chordal distance in (46) which is quite straight forward. However, cluster classification in our flag manifold using Euclidean distance given in (48) needs a deeper insight. The manifold $\mathcal{F}_{n \times n}$ consists of unique *unitary* points. For $\forall \boldsymbol{Y}_l \in \mathcal{F}_{n \times n}$, $\boldsymbol{Y}_l \in \boldsymbol{S}_i(k)$, if

$$d(\tilde{\boldsymbol{Y}}_l, \boldsymbol{Y'}_i(k)) < d(\hat{\boldsymbol{Y}}_l, \boldsymbol{Y'}_j(k)), \quad j \neq i, \quad 1 \leq j \leq N, 1 \leq i \leq N.$$

Where $\tilde{\boldsymbol{Y}}_l$ is the permuted version of $\boldsymbol{Y}_l$ w.r.t $\boldsymbol{Y'}_i$ and $\hat{\boldsymbol{Y}}_l$ is the permuted version of $\boldsymbol{Y}_l$ w.r.t $\boldsymbol{Y'}_j$

After classification, we calculate the mean quantization error $d_{\mathrm{avgdist}}(k)$ between the codeword and each training vector of the cluster associated to that codeword.

Codebook evaluation   If the decrease in the overall distortion at the current iteration $d_{\mathrm{avgdist}}(k)$ relative to previous $d_{\mathrm{avgdist}}(k-1)$ is below a certain reference threshold or no further improvement is made, then stop; otherwise goto *centroid generation*.

Centroid generation We now compute the centroid for all the given training vectors in each cluster given as

$$\boldsymbol{Y'}_i(k+1) = \mathrm{cent}(\boldsymbol{S}_\mathrm{i}(\mathrm{k})) \tag{66}$$

where $\mathrm{cent}(\boldsymbol{S}_\mathrm{i}(\mathrm{k}))$ is denoted in (57)

Centroid condition in Grassmann manifold($\mathcal{G}_{n,p}$) In this specific case the distortion metric is the chordal distance defined in (46) and the Centroid computation on the Grassmann manifold is [36]

$$\boldsymbol{Y'}_i(k+1) = \mathcal{E}_{\boldsymbol{S}_i}[d^2(\boldsymbol{Y}, Q(\boldsymbol{Y}))] \approx \arg\min_{\boldsymbol{Y}} \sum_{m=1}^{M} d^2(\boldsymbol{Y}_m, \boldsymbol{Y}) = \mathrm{eig}\left(\sum_{\mathrm{m}=1}^{\mathrm{M}} \boldsymbol{Y}_\mathrm{m}\boldsymbol{Y}_\mathrm{m}^*\right) \tag{67}$$

Where the training set vector $\boldsymbol{Y}_m \in \mathcal{G}_{n,p}$. M is the number of elements in a given cluster and eig(Z) denotes the column space of the dominant p eigenvectors of the matrix Z [36].

Centroid condition in a flag manifold ($\mathcal{F}_{n,n}$) For a given number of unitary points $\tilde{\boldsymbol{Y}}_m, 1 \le m \le M$, each column vector, $\tilde{\boldsymbol{y}}_j$ of this permuted matrix, lies in $\mathcal{G}_{n,1}$. The centroid condition in (67) is for $\mathcal{G}_{n,p}$. For $\mathcal{G}_{n,1}$, we have

$$\boldsymbol{c}_j = \mathrm{eig}\left(\sum_{\mathrm{m}=1}^{\mathrm{M}} \tilde{\boldsymbol{y}}_{\mathrm{m,j}}\tilde{\boldsymbol{y}}_{\mathrm{m,j}}^*\right); \quad 1 \le \mathrm{j} \le \mathrm{n}, \tag{68}$$

where $\boldsymbol{c}_j \in \mathcal{G}_{n,1}$ is the centroid vector[7]. For a given matrix $\boldsymbol{M} = [\boldsymbol{c}_1, ..., \boldsymbol{c}_n]$, we acquire a unitary matrix $\boldsymbol{U}_c$ via polar decomposition

$$\mathrm{polar\ decomposition}[\boldsymbol{M}] = \boldsymbol{P}\boldsymbol{U}_\mathrm{c}, \tag{69}$$

where $\boldsymbol{P}$ is a *positive semi definite Hermitian matrix* and $\boldsymbol{U}_c$ is the centroid in the flag manifold $\mathcal{F}_{n\times n}$. Hence, the updated centroid for $\boldsymbol{S}_i^{th}$ cell is

$$\boldsymbol{Y'}_i(k+1) = \boldsymbol{U}_c.$$

The following diagrams give a better understanding about the Lloyd algorithm. The Voronoi diagram of the current points at each iteration is shown, the + signs denote the centroids of the Voronoi cells.

5.3   CodeBook Constructor and Simulator

In this section, we discuss on the procedure used for codebook construction along with the parameters used with the help of a flow chart and table respectively. We begin by generating many random points over the unitary space with an initial codebook based on any heuristic. We now quantize the space and calculate new

---

[7]eig(.) here corresponds to the first dominant Eigenvector

(a) First iteration (b) Second iteration (c) Third iteration (d) n^{th} iteration
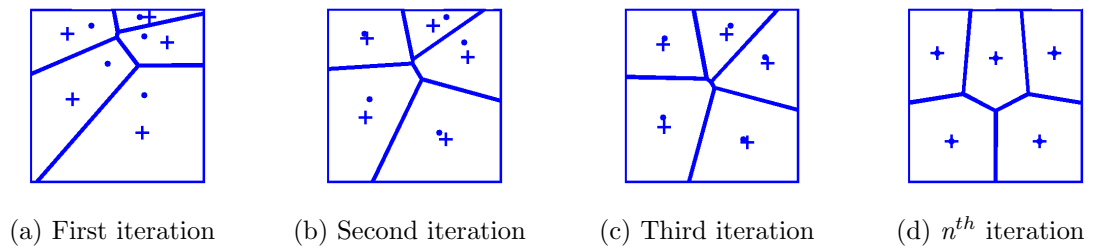
Figure 23: Distribution of codewords after succesive iterations

codewords, i.e. run Lloyd alogorithm in an iterative fashion. With every iteration, the codewords become more and more uniformly distributed. We continue until there is no further improvement in codebook which is reflected in the expected distortion. In the Monte Carlo simulations, we compare our results with the semi analytical bounds analyzing the codebook's quality. Once the codebook is obtained, we use them for transmit precoding, and analyze its impact on the system's capacity.

A generic flowchart of the system simulator is shown in Figure 24
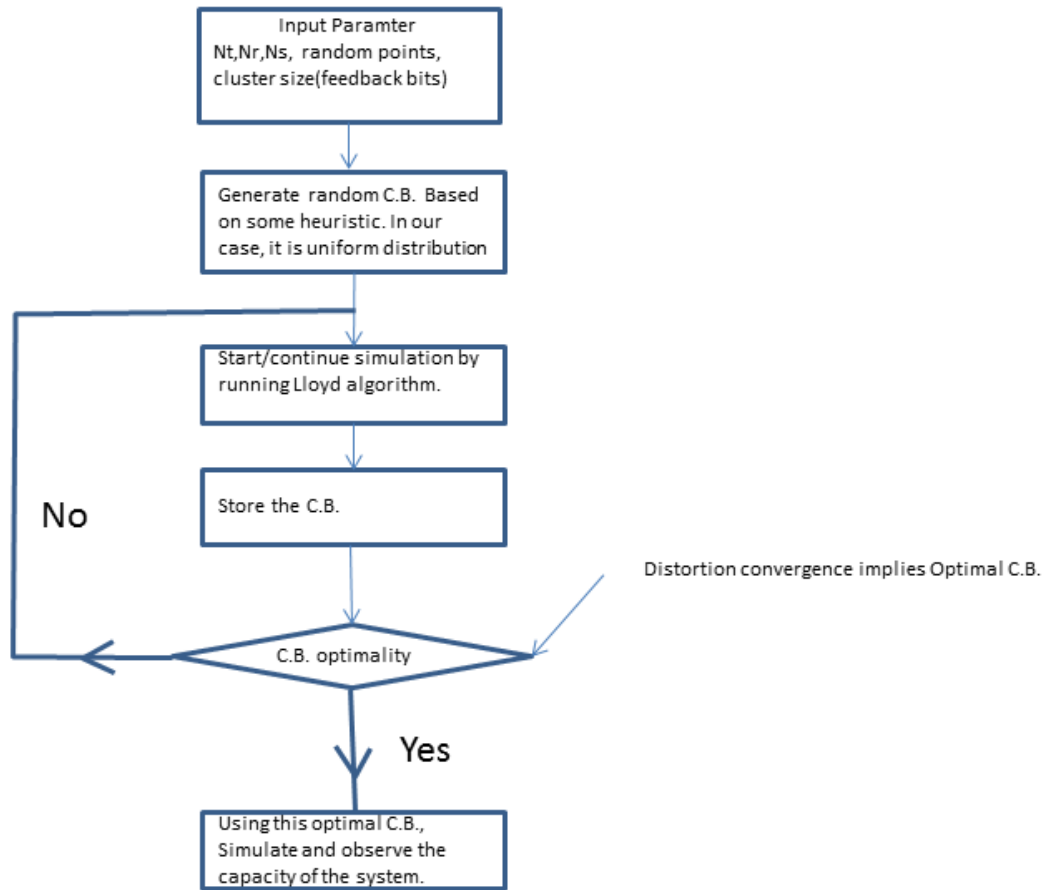

Figure 24: Flow chart of the system simulator

5.3.1   Simulation parameters

The codebook construction and simulator comprises of two parts. The first part is used to construct and evaluate the codebook, while the second part is used to analyze the impact of using this codebook on a system's throughput. Table 2 presents the simulation parameters for expected distortion.

Table 2: Distortion Simulation Parameters

Parameters	Values
Transmitters(n_T)	[2,3,4]
Spatial sub streams($n_S = \min(n_T, n_R)$)	[2,3,4]
Voronoi cells(N)	[4,6,8,16]
Random points generated	10^4

5.4 Codebook Evaluation

In this section, we present our results on Monte Carlo simulations of expected distortion, which reflects the codebook's quality. We also evaluate the codebook w.r.t the semi analytical bounds given in (64). After having validated, we discuss the factors affecting codebook's performance.

We would also like to remind the readers that this thesis mainly concerns about the codebook construction on flag manifold. However, we briefly present results for Grassmann codebook which is implemented in [48].

5.4.1 Monte Carlo Simulations

We have considered the aforementioned Lloyd algorithm to construct codebooks on $\mathcal{F}_{n \times n}$, or on unitary groups $\mathcal{U}(n)$ with different degrees of n, where $n = 2, 3, 4$. In other words, we have MIMO systems with $n_S = n_T = n_R = 2, 3, 4$ respectively. We initially generate 10^4 random points with uniform distribution. We then run the Lloyd algorithm iteratively until the expected distortion converges to a certain point signifying no more improvement in the codebook, we terminate the procedure as indicated in Figures 25, 26, 27. From the same figs, we observe that the distortion is decreasing gradually until it converges, usually around the twentieth iteration. Since the expected distortion is approaching the lower bound after convergence, we can safely infer that the codebook is indeed good, if not optimal since the bounds are obtained via numerical method.

The following Table 3 shows the numerical results obtained in Figures 25, 26, 27

5.4.2 Factors affecting Expected Distortion

A system's capacity is a function of expected distortion. So, it becomes essential to analyze the factors affecting expected distortion, which are discussed here.

Table 3: Numerical values of expected distortion with bounds

(n_T, n_R)	Number of clusters	Simulated distortion	Lower bound	Upper bound
2×2	4	0.12875	0.1278	0.13421
	6	0.0829	0.0812	0.0948
	8	0.062	0.0608	0.0698
	16	0.03	0.029	0.036
3×3	4	0.76	0.75	0.91
	6	0.65	0.649	0.88
	8	0.558	0.554	0.738
	16	0.45	0.438	0.535
4×4	4	1.52	1.42	1.92
	6	1.4	1.3	1.85
	8	1.38	1.25	1.79
	16	1.15	1.05	1.52

Codebook Size   For a given unitary space, we approximate any random point to its nearest centroid. This approximation, or quantization of $\mathcal{U}(n)$ brings about a distortion. When the volume of a given cluster is large then the error in approximation is also large. In order to minimize this error we increase the number of clusters minimizing the volume of each cluster effectively reducing the average distortion as illustrated in Figures 28, 29.

$$N_f = \log_2(N_{\text{clusters}}),$$

where N_f, N_{clusters} are number of feedback bits and clusters respectively. When
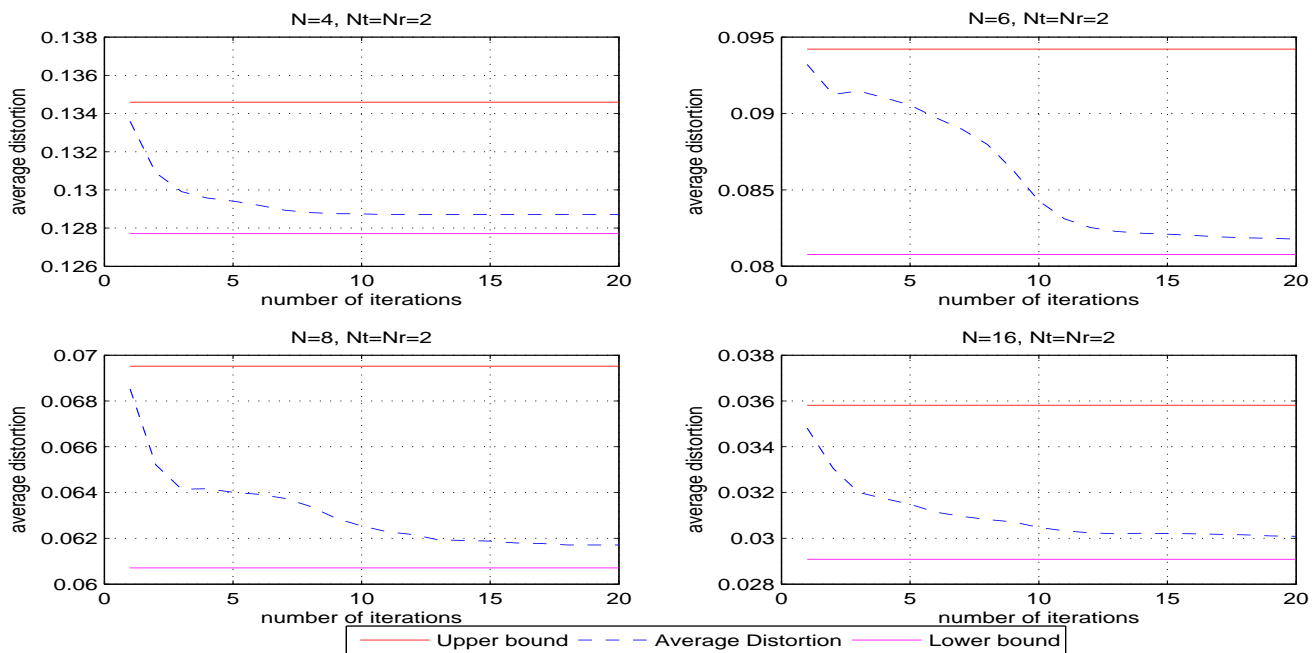
Figure 25: Simulated expected distortion analytically bounded for a 2×2 MIMO.
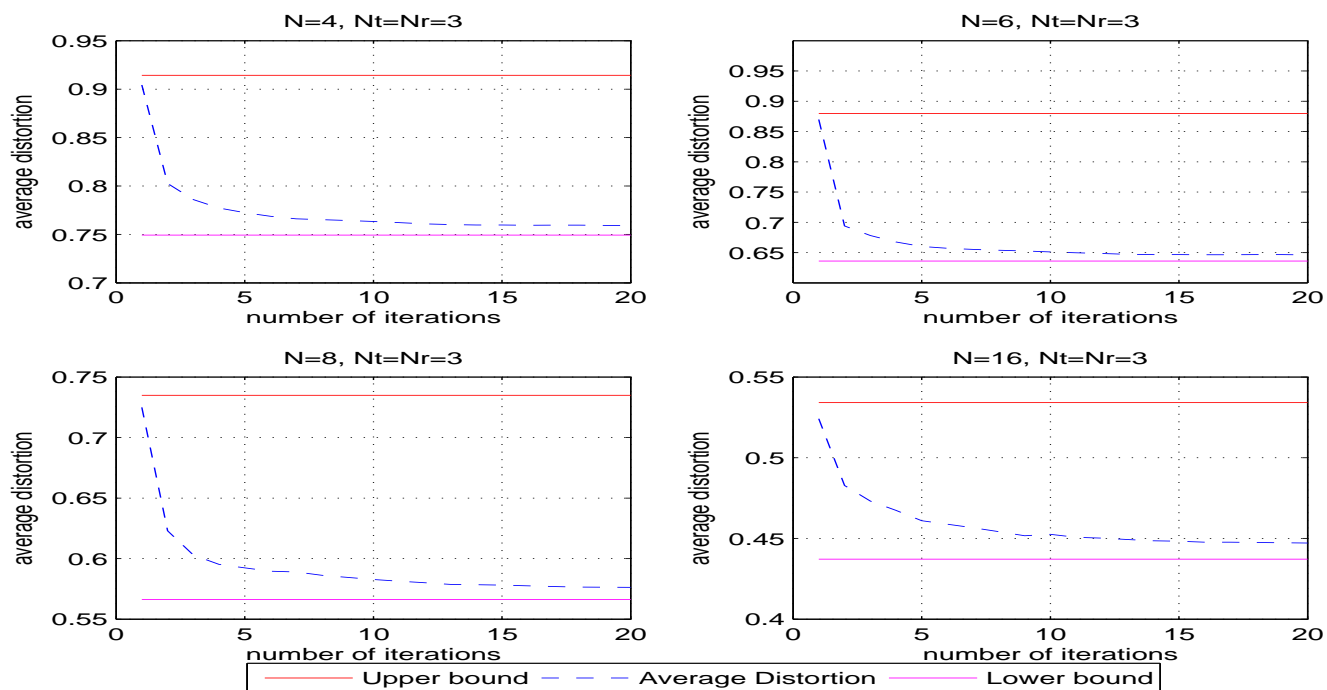

Figure 26: Simulated expected distortion analytically bounded for a 3×3 MIMO.
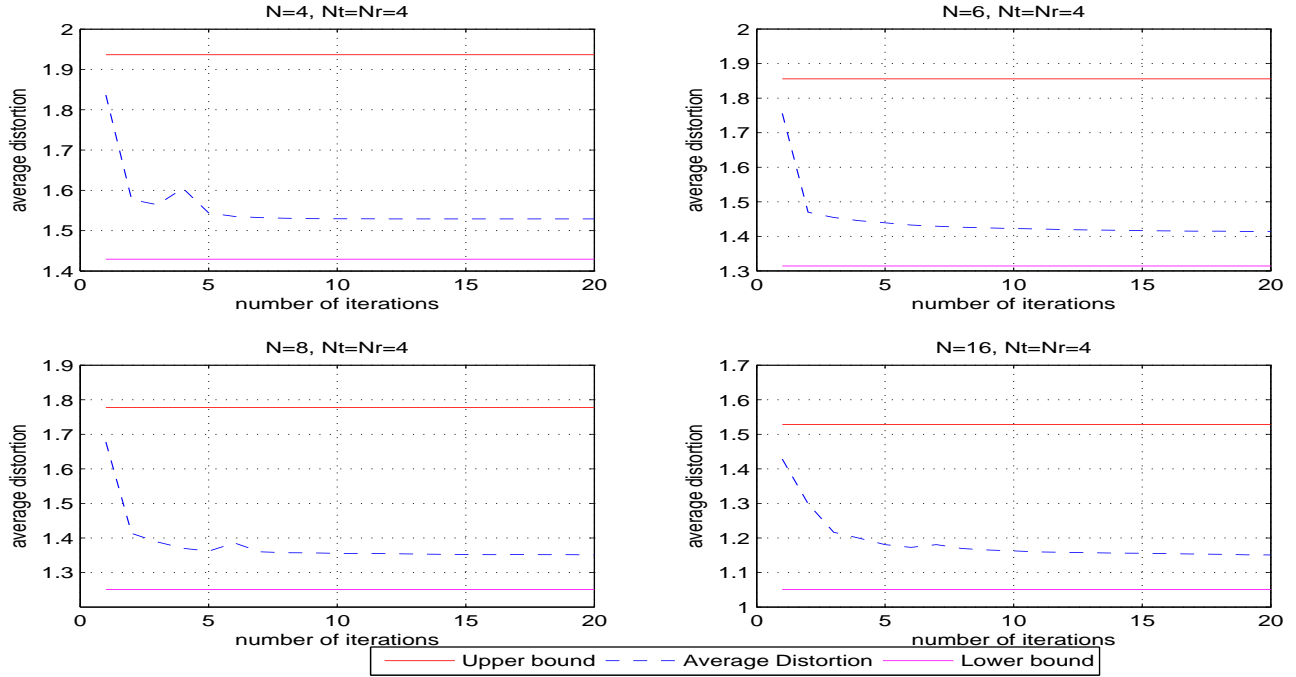
Figure 27: Simulated expected distortion analytically bounded for a 4×4 MIMO.

more bits are fed back, the transmitter has more codewords in the codebook to choose from. In other words, it can have a better approximation, and combat the channel $\boldsymbol{H}$ efficiently.

Impact of Spatial Sub-streams   The increase in spatial sub-streams results in degradation of expected distortion, irrespective of the codebook used. We have two codebooks; from the flag manifold, Grassmann manifold as shown in Figures 28, 29 respectively. The flag manifold codebook is used when $n_S = n_T = n_R$, and the Grassmann codebook is used when $n_S = \min(n_T, n_R)$. For a certain number of spatial sub-streams, the Grassmann codebook yields a better performance than the flag manifold codebook. We observe that $\mathcal{G}_{4,2}$ in Figure 29 yields a lesser distortion than $\mathcal{F}_{2,2}$ in Figure 28. This is more apparent in the capacity simulations presented in the next section. In any case, this effect of distortion can be combated by increasing codebook cardinality.
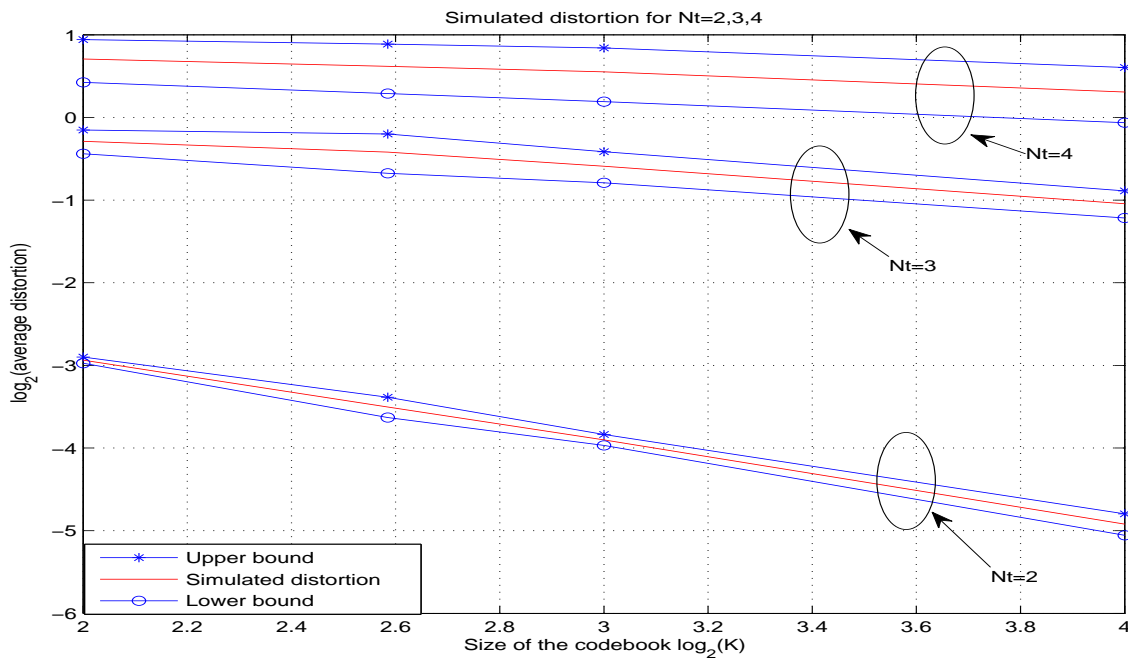
Figure 28: Codebook evaluation as a function of expected distortion for Riemannian manifold.
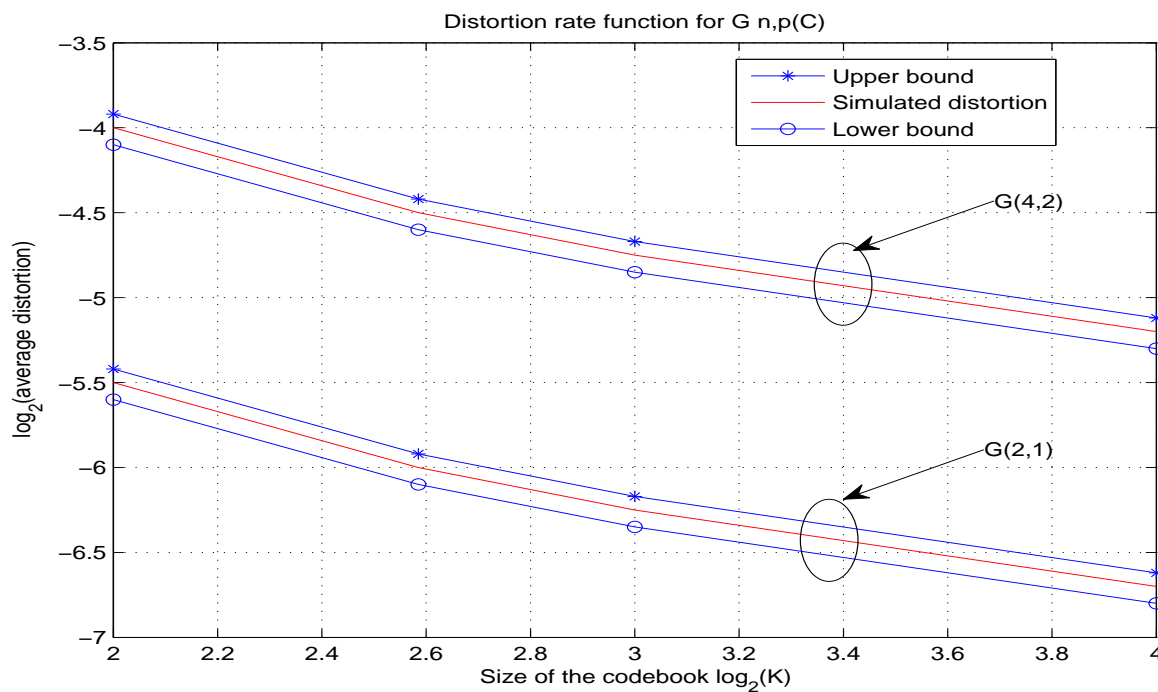

Figure 29: Codebook evaluation as a function of expected distortion for Grassmann manifold

5.5   Exhaustive Search Technique

We further analyze the proposed codebook's performance by comparing it with codebook designed via brute force method. The problem of finding a *centroid candidate* in a uniformly distributed space of *unitary* points can be solved by brute force method in which we generate many points and test its accuracy as a centroid candidate[8]. This is a trivial problem solving technique which requires high computation, and is generally not feasible. However, we use this method to evaluate our codebook's quality obtained via Monte Carlo simulations.

For a given number of unitary points in a cluster, we begin our exhaustive search by selecting a random point in the cluster as a centroid candidate minimizing the distortion. We increase the sample size of these random points and repeat the process until the sample size contains all the unitary points distributed over the cluster. We then compare this centroid candidate with the proposed centroid obtained via Monte Carlo simulations. In Figure 30, 31, 32, we observe that exhaustive search distortion is decreasing with the increase in sample size but is never better than the proposed distortion. This suggests the centroid obtained via Lloyd algorithm is better than any random point generated in the cluster.
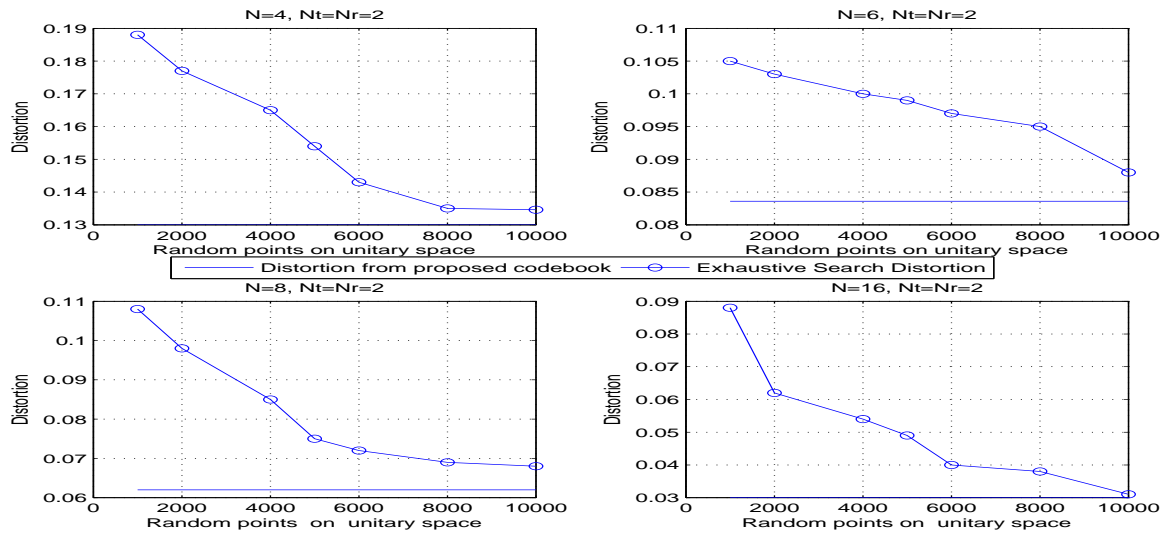
Figure 30: Estimation of numerically obtained centroid against brute force method for 2×2 MIMO system

The other observation that can be made is in the decrease of proposed distortion with increase in the number of clusters(or feedback bits), i.e.$N = 4, 6, 8, 16$, for a fixed MIMO system. Which can be seen from Figure 30, 31, 32 respectively and is summarized in Table 3. For a given space, the increase in number of clusters

---

[8]The terms centroid, distortion, codebook are interchangeable in context of performance as they are all linearly related
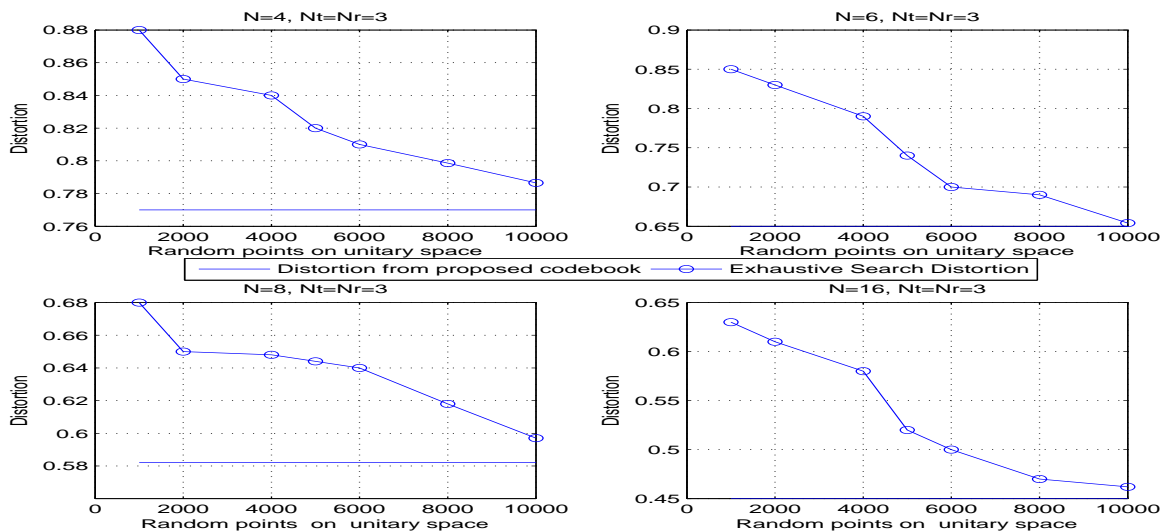
Figure 31: Estimation of numerically obtained centroid against brute force method for 3×3 MIMO system.
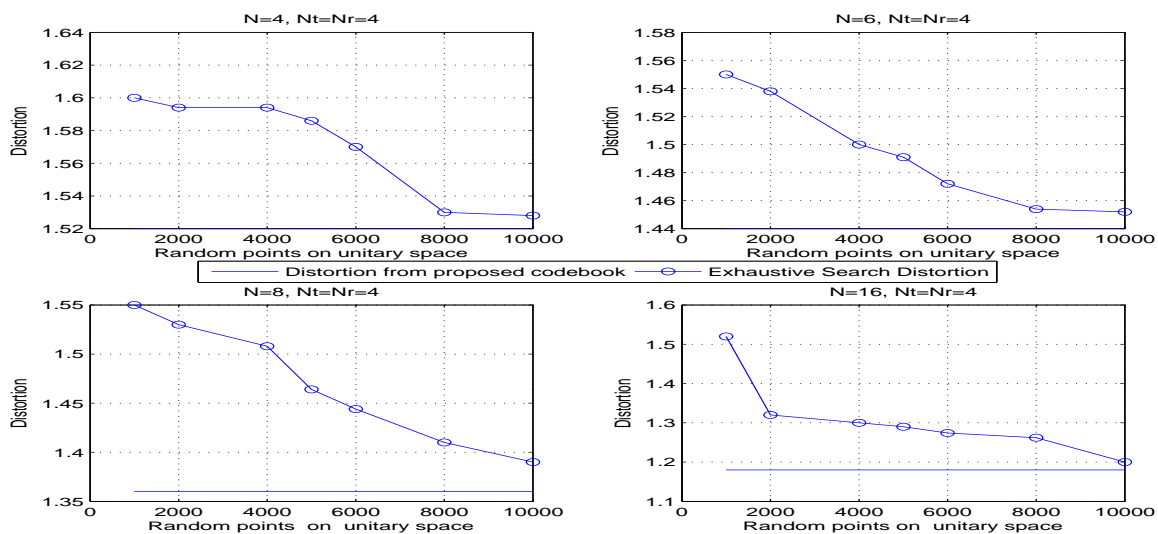
Figure 32: Estimation of numerically obtained centroid against brute force method for 4×4 MIMO system.

will effectively reduce the volume of each cluster, thereby reducing any outliers, facilitating a better quantization process. However, this physically results in more feedback bits from receiver to the transmitter. From the exhaustive search test, we can infer that the proposed codebook fairs better than any other codebook constructed via any random search.

6 Capacity Analysis for Limited Feedback MIMO systems with Linear Receiver

In the previous section, we constructed our codebook used in transmit precoding. In this section, we mainly present our capacity simulations addressing the scope of the thesis.

6.1 Linear Receivers

One aspect that makes linear receivers unique is the methodology of using a linear filter to separate each of the distinct spatial sub-streams. This filter is represented by a weighted matrix $\boldsymbol{Z}$. The vector estimate, $\tilde{\boldsymbol{y}}$ is given by

$$\tilde{\boldsymbol{y}} = \boldsymbol{Z}\boldsymbol{y} = \boldsymbol{Z}\boldsymbol{H}_{\text{eq}}\boldsymbol{x} + \boldsymbol{Z}\boldsymbol{w}. \tag{70}$$

$\boldsymbol{H}_{\text{eq}} = \boldsymbol{H}\boldsymbol{M} = \boldsymbol{U}_{\text{eq}}\boldsymbol{\Lambda}_{\text{eq}}\boldsymbol{V}_{\text{eq}}^*$, where $\boldsymbol{M}$ is the codeword used at the transmitter, $\boldsymbol{V}_{\text{eq}}$ are the right singular vectors and $\boldsymbol{\Lambda}_{\text{eq}}$ contains the singular values. We also define

$$\boldsymbol{R}_{\text{eq}} = \boldsymbol{H}_{\text{eq}}^*\boldsymbol{H}_{\text{eq}}$$

as the equivalent correlation matrix [42].

6.1.1 Zero Forcing Equalizer

The zero forcing equalizer involves a simple linear filter scheme, aims at eliminating interference between each independent sub-stream originating from each of the multiple transmit antennas [49]. This is facilitated by computing the Moore-Penrose pseudo-inverse of the equivalent channel matrix [50, page 210], and setting it to $\boldsymbol{Z}$

$$\boldsymbol{Z} = (\boldsymbol{H}_{\text{eq}}^*\boldsymbol{H}_{\text{eq}})^{-1}\boldsymbol{H}_{\text{eq}}^*,$$

However, one of the downsides of ZF receivers is that they suffer from noise enhancement [51].

Assuming that the receiver has complete channel knowledge, (70) is modified to

$$\tilde{\boldsymbol{y}} \quad = \quad (\boldsymbol{H}_{\text{eq}}^*\boldsymbol{H}_{\text{eq}})^{-1}\boldsymbol{H}_{\text{eq}}^*\boldsymbol{H}_{\text{eq}}\boldsymbol{x} + \boldsymbol{Z}\boldsymbol{w} \quad = \quad \boldsymbol{x} + \boldsymbol{Z}\boldsymbol{w} \tag{71}$$

The purpose of transmit precoding is to increase the capacity(or spectral efficiency) of the system. We modify the capacity expression in (30) to

$$C = \log_2 \det\left(\boldsymbol{I}_{n_R} + \gamma\boldsymbol{R}_{\text{eq}}\right), \tag{72}$$

where $\gamma = \frac{P_s}{n_S\sigma^2}$, in the absence of water filling $\boldsymbol{Q} = \boldsymbol{I}$. However, we are using a ZF linear receiver and reaching the optimum capacity is not possible unless the correlation matrix, $\boldsymbol{R}_{\text{eq}}$ is a diagonal matrix. Alternatively for a linear receiver, the general throughput equation can be written as [42]

$$C = \sum_{i=1}^{n_S} \log_2(1 + \gamma_i), \tag{73}$$

where γ_i is the post-processing SINR of the ith data stream given by

$$\gamma_i = \frac{1}{\boldsymbol{Z}\mathcal{E}\{\boldsymbol{w}\boldsymbol{w}^*\}\boldsymbol{Z}^*} = \frac{1}{\sigma_n^2 \boldsymbol{Z}\boldsymbol{Z}^*} = \frac{1}{[\gamma \boldsymbol{R}_{\text{eq}}]_{i,i}^{-1}}.$$

We have simulated the capacity results for different MIMO scenarios. We analyze the impact of feedback bits, low and high regions of SNR, and spatial sub-streams on these systems.

6.2 Impact of Feedback Bits and Average Received SNR

We have previously seen the impact of codebook size on the expected distortion. As mentioned earlier, the system capacity, which is a function of distortion also gets affected. The system's channel is denoted by a full rank matrix with equal number of transmit and receive antennas. Figure 33, 34, 35 shows the flow of information for 2×2, 3×3, and 4×4 systems respectively. Since we are using a ZF equalizer, information rate is dependent on precoding unlike the maximum likelihood receiver. For a 2×2 MIMO system, we require only few feedback bits to approach perfect precoding as illustrated in Figure 33. However, this is not the case in higher order systems because with the increase in antennas, the volume of flag manifold becomes large requiring more Voronoi cells(or feedback bits) to quantize the unitary space, affecting the codebook's performance. Thus, from Figure 34, 35, we can see system throughput becomes more and more immune to precoding.

The same can be observed while using Grassmann precoding as shown in Figure 36, where $\mathcal{G}_{2,1}$ requires only 2 feedback bits to approach perfect precoding and system performance degrades with the increase in the number of spatial sub streams as seen in $\mathcal{G}_{4,2}$. The additional knowledge of channel available at the transmitter facilitates us to allocate different power levels to the transmitters based on water filling concept further increasing the system capacity.

6.3 Impact of Spatial sub-streams

There is a fundamental trade off between spatial multiplexing and diversity gain. Increasing the spatial sub-streams, we increase the system capacity at the cost of diversity. However, in the case of unitary precoding with higher sub-streams($n_S = n_T = n_R$), the relative gain becomes small and the improvement is slow as shown in Figure 33 and Figure 35. The impact of precoding is adversely affected, eventually leading to no improvement in the performance.
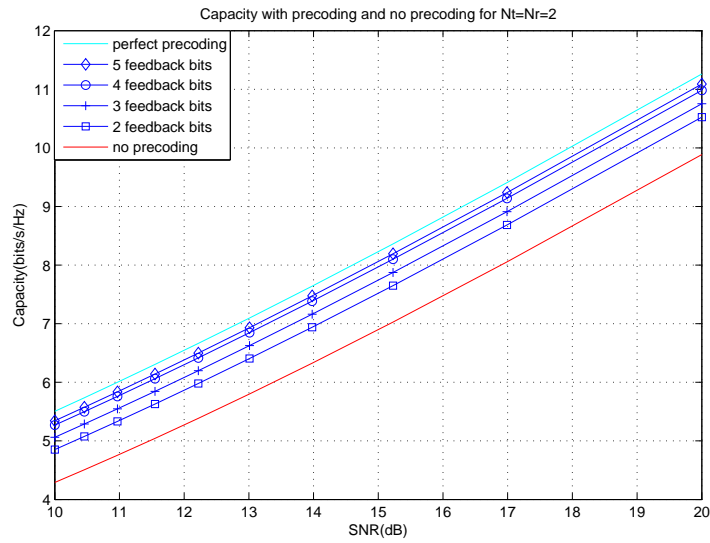
Figure 33: Capacity for a 2×2 system using unitary precoding.
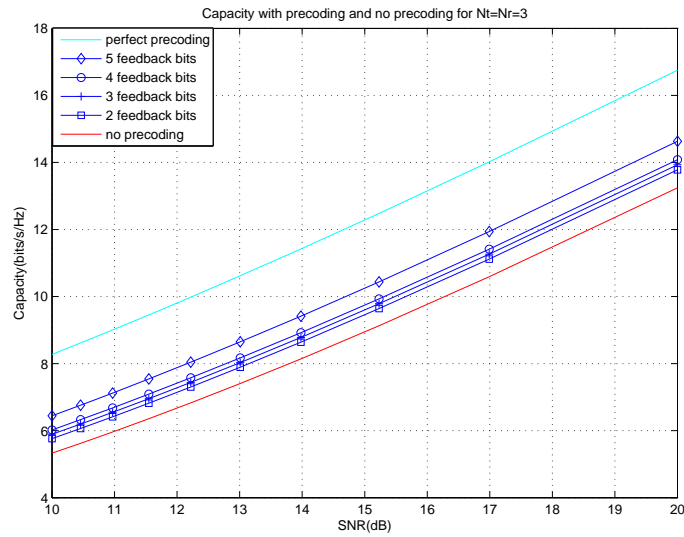

Figure 34: Capacity for a 3×3 system using unitary precoding.
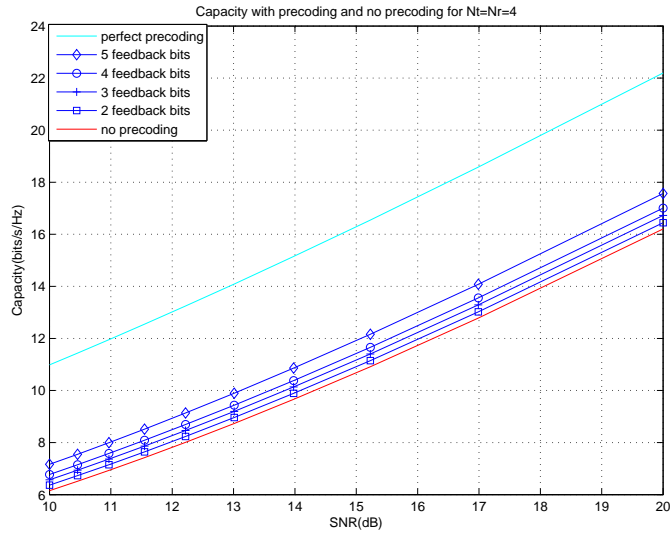
Figure 35: Capacity for a 4×4 system using unitary precoding.
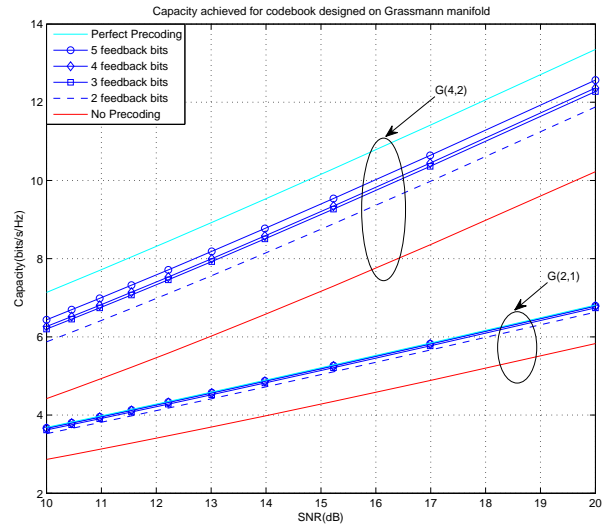
Figure 36: Capacity of a 2×1 and 4×2 MIMO system using Grassmann precoding.

For a given number of spatial sub-streams, Grassmann precoding $\mathcal{G}_{4,2}$ performs better in terms of system capacity, having a gain of almost 3dB over unitary precoding $\mathcal{F}_{2,2}$ as illustrated in Figure 36, Figure 33 respectively. For higher sub streams, quantizing unitary space is not a trivial task due to it's large volume, which is reflected in the system performance.

6.4 Impact of Codebook Partition on Capacity

We have designed codebooks in two different scenarios. In the first scenario, we introduce a quantization scheme in which the full space of non-equivalent precoding matrices is a flag manifold($\mathcal{F}_{n,p}$). While in the second scenario, the same space is partitioned into Grassmannian part($\mathcal{G}_{n,p}$) and unitary group($\mathcal{F}_{p,p}$). We have simulated and compared the capacities for both scenarios in Figure 37.

6.4.1 Codebook Partitioning

We partition the precoding matrix $\boldsymbol{M}$ into a part $\boldsymbol{G}$ corresponding to a point in the Grassmann manifold $\mathcal{G}_{n,p}$ and point $\boldsymbol{O}$ in the unitary space $\mathcal{F}_{p,p}$.

$$\boldsymbol{M} = \boldsymbol{GO},$$

The transmitted symbols can be interchanged. This means that orthogonalization matrices that are column permutations of each other are equivalent. The overall phases of the columns are irrelevant. Thus, the space of non-equivalent orthogonalization matrices occupy the coset space [42]

$$\mathcal{F}_{p,p} = \mathcal{U}_p/(\mathcal{P}_p \times \mathcal{U}_1^p).$$

The orthogonal matrices are equivalent up to a p-fold direct product of p phases and and the set of column permutations forming the permutation group of p elements, $\mathcal{P}_p$. The orthogonalization part of the precoding matrix $\boldsymbol{M}$ is independent of the metric used in Grassmannian space.

6.4.2 Capacity Analysis

Figure 37 illustrates the achievable data rate for a 4×2 MIMO system using a ZF equalizer with 2 spatial sub-streams. The code book is designed on $\mathcal{F}_{4,2}$ and $\mathcal{G}_{4,2}$. It is quite evident from the figure that flag manifold codebook is achieving the data rate which is almost equal to the optimum, better than Grassmann precoding, $\mathcal{G}_{4,2}$. The codebook designed by partitioning the space into $\mathcal{G}_{4,2}$ and $\mathcal{F}_{2,2}$ [42], each having two bits gives an intermediate performance between the two. The design criteria for the codewords selection is based on minimizing the flag distance jointly over all the possible combinations of Grassmannian and orthogonalization codewords.
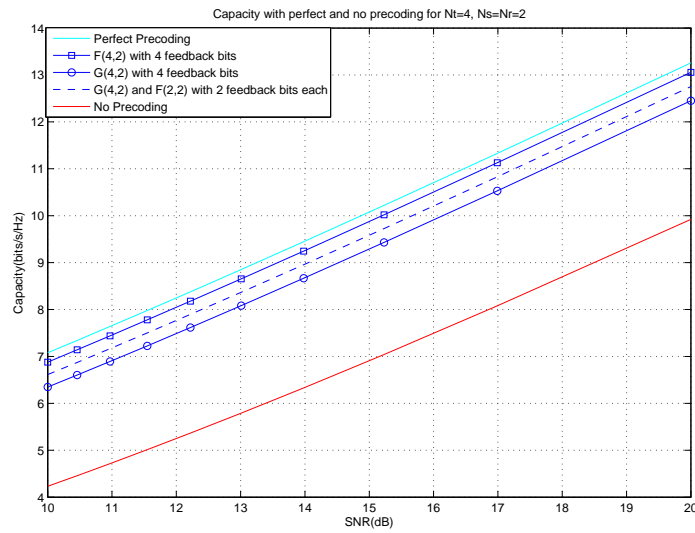
Figure 37: Codebook performance with/without precoder partitioning.

7 Conclusions and Future Work

7.1 Conclusions

Codebooks are employed in MIMO wireless systems with the intention of acquiring partial CSIT in order to achieve higher data rates. The work done during this thesis mainly concerns with the design of these codebooks. The designing of codebooks is closely related to quantizing aforementioned manifolds.

As a background, the evolution of MIMO systems from a simple SISO system is reviewed along with its many advantages. Some classical information theory concepts concerning capacity were presented with derivations for corresponding capacity of a MIMO system, which is used later in our simulations and performance analysis. The prerequisites of codebook designing are manifolds and quantization principles which are explained in sections 3 and 4 respectively.

A matlab simulator was built to design our codebook using Lloyd algorithm to quantize our manifolds. In Section 5, simulation results were presented with respect to codebook design aspect: validation of our centroid estimate, simulated expected distortion with its corresponding analytical bounds, impact of feedback bits and rank of MIMO system on expected distortion. These Monte Carlo simulations confirms the codebook's optimality.

Finally, simulations on capacity for a limited feedback MIMO system are presented in Section 6. These simulations confirms the improvement in achievable data rates due to precoding. The main conclusions that were drawn from this thesis are: Increase in number of feed back bits improves the capacity of a system, increase in spatial sub-streams adversely affects the feedback bits' effect on the capacity. Codebook designed by quantizing flag manifold without partition yields a better performance when compared to the codebook obtained by partitioning the space into Grassmannian and orthogonalization parts.

7.2 Future work

Future work could include a better mathematical analysis of the manifolds, as the distortion bounds derived are not completely tight; The distortion bounds derived in Section 5 are sub optimal. In Section 6, it would be justifiable to have capacity bounds as a function of distortion instead of perfect and no precoding, since it would give a better analysis on the performance of a system. The channel considered in this thesis has been i.i.d., one suggestion would be to use a correlated channel and analyze the performance.

Appendices

Polar Decomposition

The polar decomposition is employed to obtain a unitary matrix, $\boldsymbol{U}$ and a positive-semidefinite Hermitian matrix, $\boldsymbol{P}$. For any given square complex matrix $\boldsymbol{A}$. The S.V.D of the given matrix $\boldsymbol{A}$ yields $\boldsymbol{W\Lambda V}^*$. we now have the relation

$$\boldsymbol{U} = \boldsymbol{WV}^*, \quad \boldsymbol{P} = \boldsymbol{W\Lambda W}^*$$

Lie Groups

The aforementioned unitary group, $\mathcal{U}_n$ is a Lie group. A Lie group $\boldsymbol{G}$ is a set that is (a) A group in the usual algebraic sense;

(b) A differentiable manifold with the properties that taking the product of two group elements, and taking the inverse of a group element, are smooth operations devoid of any singular points. Specifically the multiplication maps $\boldsymbol{G} \times \boldsymbol{G} \to \boldsymbol{G}$

$$(\boldsymbol{g}_1, \boldsymbol{g}_2) \mapsto \boldsymbol{g}_1\boldsymbol{g}_2$$

and the inverse $\boldsymbol{G} \to \boldsymbol{G}$

$$\boldsymbol{g} \mapsto \boldsymbol{g}^{-1}$$

are $\boldsymbol{C}^\infty$.

The skew-Hermitian group forms the corresponding Lie algebra to the unitary group, $\mathbf{u}_n$. The Lie algebra encodes many of the properties of its corresponding Lie group, its underlying vector space is the tangent space of the group at the identity element, which completely captures the local structure of the group. A point from Lie algebra can be mapped to its Lie group via exponential mapping .

References

[1] D. Tse and P. Viswanath, *Fundamentals of Wireless Communication.* New York: Cambridge University Press, 2005.

[2] I. Telatar, "Capacity of Multi-antenna Gaussian Channels," *European Transactions on Telecommunications.*

[3] M. Wrulich, "Capacity analysis of MIMO systems," Master's thesis, TU Vienna, Jan. 2006.

[4] P. Xia and G. Giannakis, "Design and analysis of transmit-beamforming based on limited-rate feedback," *IEEE Transactions on Signal Processing*, vol. 54, pp. 1853 – 1863, May 2006.

[5] P. Almers, E. Bonek, A. Burr, N. Czink, M. Debbah, V. Degli-Esposti, H. Hofstetter, P. Kyösti, D. Laurenson, G. Matz, A. F. Molisch, C. Oestges, and H. Özcelik, "Survey of channel and radio propagation models for wireless MIMO systems," *EURASIP Journal on Wireless Communication and Networking*, vol. 2007, pp. 56–56, Jan. 2007.

[6] B. Vucetic and J. Yuan, *Space-Time coding.* Chichester: Wiley publications, 2003.

[7] J. Steele, *The Cauchy-Schwarz Master Class: The Art of Mathematical Inequalities.* New York: Cambridge University Press, 2004.

[8] V. Tarokh, N. Seshadri, and A. Calderbank, "Space-time codes for high data rate wireless communication: performance criterion and code construction," *IEEE Transactions on Information Theory*, vol. 44, pp. 744 –765, Mar. 1998.

[9] A. Naguib and R. Calderbank, "Space time coding and signal processing for high data rate wireless communications," *IEEE Signal Processing Magazine*, vol. 17, no.3, pp. 76–92, Mar. 2000.

[10] J. Winters, "Switched diversity with feedback for DPSK mobile radio systems," *IEEE Transactions on Vehicular Technology*, vol. 32, pp. 134 – 150, Feb. 1983.

[11] G. J. Foschini and M. J. Gans, "On Limits of Wireless Communications in a Fading Environment when using Multiple Antennas," *Wireless Personal Communications*, vol. 6, pp. 311–335, Mar. 1998.

[12] S. Muller-Weinfurtner, "Coding approaches for multiple antenna transmission in fast fading and OFDM," *IEEE Transactions on Signal Processing*, vol. 50, pp. 2442 – 2450, Oct. 2002.

[13] T. Cover and J. Thomas, *Elements of Information Theory.* Hoboken: John wiley & Sons, 2006.

[14] M. Jankiraman, *Space-time codes and MIMO systems.* Boston: Artech house universal personal communications library, 2004.

[15] D. A. Harville, *Matrix Algebra From a Statistician's Perspective.* New York: Springer, 1997.

[16] A. Hottinen, O. Tirkkonen, and R. Wichman, *Multi-antenna Transceiver Techniques for 3G and Beyond.* John Wiley & Sons Ltd., 2003.

[17] A. Goldsmith, S. Jafar, N. Jindal, and S. Vishwanath, "Capacity limits of MIMO channels," *IEEE Journal on Selected Areas in Communications*, vol. 21, pp. 684 – 702, Jun. 2003.

[18] L. Zheng and D. Tse, "Diversity and multiplexing: a fundamental tradeoff in multiple-antenna channels," *IEEE Transactions on Information Theory*, vol. 49, pp. 1073 – 1096, May 2003.

[19] G. Foschini, "Layered space-time architecture for wireless communication in a fading environment when using multi-element antennas," *Bell Labs Technical Journal*, vol. 1, pp. 41–59, 1996.

[20] D. W. Bliss, K. W. Forsythe, A. O. Hero, III, and A. F. Yegulalp, "Environmental Issues for MIMO Capacity," *IEEE Transactions Signal Processing*, vol. 50, pp. 2128–2142, 2002.

[21] H. Bolcskei and A. Paulraj, "Performance of space-time codes in the presence of spatial fading correlation," in *Asilomar Conference on Signals, Systems and Computers*, vol. 1, pp. 687 –693, Nov. 2000.

[22] Y. J. Cho, R. Saadati, and S. Wang, "Common fixed point theorems on generalized distance in ordered cone metric spaces," *Computers & Mathematics with Applications*, vol. 61, pp. 1254–1260, Feb. 2011.

[23] S. Lang, *Introduction to Differentiable Manifolds.* Springer, 2002, second edition.

[24] C. J. Isham, *Modern Differential Geometry for Physicists.* World Sceintific Publishing Co. Re. Ltd, 2001, second edition, vol. 61.

[25] M. Heller, L. Pysiak, and W. Sasin, "Geometry of non-Hausdorff spaces and its significance for physics," *Journal of Mathematical Physics*, vol. 52, no. 4, p. 043506, 2011.

[26] J. D. Wine, "Extending Expansive Homeomorphisms," *Proceedings of the American Mathematical Society*, vol. 86, no. 3, pp. 531–534, 1982.

[27] G. B. Thomas and R. L. Finney, *Calculus and Analytic Geometry.* Delhi: Pearson Education, 2003.

[28] J. M. Lee, *Introduction to Smooth Manifolds.* New York: Springer, 2003.

[29] R. L. Bishop and R. J. Crittenden, *Geometry of Manifolds*. New York: Academic Press, 1964.

[30] X. Pennec, "Intrinsic Statistics on Riemannian Manifolds: Basic Tools for Geometric Measurements," *Journal of Mathematical Imaging and Vision*, vol. 25, no. 1, pp. 127–154, 2006.

[31] J.-P. Dedieu and D. Nowicki, "Symplectic methods for the approximation of the exponential map and the Newton iteration on Riemannian submanifolds," *Journal of Complexity*, vol. 21, pp. 487–501, Aug. 2005.

[32] L. Zheng and D. Tse, "Communication on the Grassmann manifold: a geometric approach to the noncoherent multiple-antenna channel," *IEEE Transactions on Information Theory*, vol. 48, pp. 359 –383, Feb. 2002.

[33] P.-A. Absil, R. Mahony, and R. Sepulchre, "Riemannian geometry of Grassmann manifolds with a view on algorithmic computation," *Acta Applicandae Mathematicae*, vol. 80, no. 2, pp. 199–220, 2004.

[34] W. Boothby, *An Introduction to Differential Manifolds and Riemannain Geometry*. San Diego: Academic, 2nd edition, 1986.

[35] A. Edelman, T. A. Arias, and S. T. Smith, "The geometry of algorithms with orthogonality constraints," *SIAM Journal on Matrix Analysis and Applications*, vol. 20, no. 2, pp. 303–353, 1998.

[36] B. Mondal, S. Dutta, and R. Heath, "Quantization on the Grassmann Manifold," *IEEE Transactions on Signal Processing*, vol. 55, pp. 4208 –4216, Aug. 2007.

[37] I. Kim, S. Park, D. Love, and S. Kim, "Improved multiuser MIMO unitary precoding using partial channel state information and insights from the Riemannian manifold," *IEEE Transactions on Wireless Communications*, vol. 8, pp. 4014 –4023, Aug. 2009.

[38] O. Henkel, "Sphere-packing bounds in the Grassmann and Stiefel manifolds," *IEEE Transactions on Information Theory*, vol. 51, pp. 3445 –3456, Oct. 2005.

[39] E. Akay, E. Sengul, and E. Ayanoglu, "Performance analysis of beamforming for MIMO OFDM with BICM," in *IEEE International Conference on Communications, 2005*, vol. 1, pp. 613 – 617, May 2005.

[40] A. Gersho, "On the structure of vector quantizers," *IEEE Transactions on Information Theory*, vol. 28, pp. 157 – 166, Mar. 1982.

[41] A. Gersho and R. M. Gray, *Vector Quantization and Signal Compression*. Boston: Kluwer Academic Publishers, 1992.

[42] H.-L. Maattanen, K. Schober, O. Tirkkonen, and R. Wichman, "Precoder partitioning in closed-loop MIMO systems," *IEEE Transactions on Wireless Communications*, vol. 8, pp. 3910 –3914, Aug. 2009.

[43] J. M. Lee, *Riemannian Manifolds: An Introduction to Curvature*. Springer, 1997.

[44] R. T. Krishnamachari, *Analyzing Finite-Rate Feedback of the General Covariance Matrix: Rate-Distortion and Capacity Difference Aspects*. PhD thesis, University of Colorado - Boulder, 2010.

[45] R. Krishnamachari and M. Varanasi, "Volume of geodesic balls in the complex Stiefel manifold," in *46th Annual Allerton Conference on Communication, Control, and Computing*, pp. 902 –909, Sept. 2008.

[46] W. Dai, Y. Liu, and B. Rider, "Quantization bounds on Grassmann manifolds and applications to MIMO communications," *IEEE Transactions on Information Theory*, vol. 54, pp. 1108 –1123, Mar. 2008.

[47] F. Cao, M. Sandell, and F. Tosato, "A codebook with low complexity for limited feedback precoding," in *IEEE 20th International Symposium on Personal, Indoor and Mobile Radio Communications*, pp. 1302 –1306, Sept. 2009.

[48] A. Srinivasan, "Lloyds algorithm for codebook design in MIMO wireless systems." S-72.3120, Aalto University, Oct. 2011.

[49] R. Bohnke, D. Wubben, V. Kuhn, and K.-D. Kammeyer, "Reduced complexity MMSE detection for BLAST architectures," in *IEEE Global Telecommunications Conference*, vol. 4, pp. 2258 – 2262, Dec. 2003.

[50] A. Paulraj, R. Nabar, and D. Gore, *Introduction to Space-Time Wireless Communications*. New York: Cambridge University Press, 2003.

[51] A. Benjebbour, H. Murata, and S. Yoshida, "Comparison of ordered successive receivers for space-time transmission," in *IEEE VTS 54th Vehicular Technology Conference*, vol. 4, pp. 2053 –2057, 2001.